The Importance of Size Ranges in Aerosol Instrument Intercomparisons: A Case Study for the ATom Mission

Hongyu Guo[1,2], Pedro Campuzano-Jost[1,2], Benjamin A. Nault[1,2], Douglas A. Day[1,2], Jason C. Schroder[1,2,*], Jack E. Dibb[3], Maximilian Dollner[4], Bernadett Weinzierl[4], and Jose L. Jimenez[1,2]

[1]Department of Chemistry, University of Colorado Boulder, Boulder, CO, 80309, USA
[2]Cooperative Institute for Research in Environmental Sciences, University of Colorado Boulder, Boulder, CO, 80309, USA
[3]Earth Systems Research Center, Institute for the Study of Earth, Oceans, and Space, Univ. of New Hampshire, Durham, NH, 03824, USA
[4]Faculty of Physics, University of Vienna, Vienna, Austria
[*]Now at Air Pollution Control Division, Colorado Department of Public Health and Environment, Denver, CO, 80246, USA
Correspondence to: Jose L. Jimenez (jose.jimenez@colorado.edu)

Abstract. Aerosol intercomparisons are inherently complex, as they convolve instrument-dependent detection efficiencies vs. size (which often change with pressure, temperature, or humidity) and variations on the sampled aerosol population, in addition to differences in chemical detection principles (e.g., including inorganic-only nitrate vs. inorganic plus organic nitrate for two instruments). The NASA Atmospheric Tomography Mission (ATom) spanned four separate aircraft deployments, which sampled the remote marine troposphere from 86°S to 82°N over different seasons with a wide range of aerosol concentrations and compositions. Aerosols were quantified with a set of carefully characterized and calibrated instruments, some based on particle sizing and some on composition measurements. This study aims to provide a critical evaluation of the size-related factors impacting aerosol intercomparisons, and of aerosol quantification during ATom, with a focus on the Aerosol Mass Spectrometer (AMS). The volume determined from physical sizing instruments is compared in detail with that derived from the chemical measurements of the AMS and the Single Particle Soot Photometer (SP2). Special attention was paid to characterize the upper end of the AMS size-dependent transmission with in-field calibrations, which we show to be critical for accurate comparisons across instruments with inevitably different size cuts. Observed differences between campaigns emphasize the importance of characterizing AMS transmission for each instrument and field study for meaningful interpretation of instrument comparisons. Good agreement was found between the composition-based volume (including AMS-quantified sea salt) and that derived from the size spectrometers. The very clean conditions during most of ATom resulted in substantial statistical noise (i.e., precision error), which we show to be substantially reduced by averaging at several-minute time intervals. The AMS captured, on average, $95 \pm 15\%$ of the standard PM_1 volume. These results support the absence of significant unknown biases and the appropriateness of the accuracy estimates for AMS total mass/volume for the mostly aged air masses encountered in ATom. The particle size ranges that contribute chemical composition information to the AMS and complementary composition instruments are investigated, to inform their use in future studies.

1 Introduction

Aerosols are ubiquitous in the atmosphere and have a lifetime of about a week, and thus can travel long distances (Tsigaridis et al., 2014), and have important effects on climate forcing, through both direct (Pilinis et al., 1995; Haywood and Boucher, 2000) and indirect effects (Lohmann and Feichter, 2005; IPCC, 2013). Remote regions account for much of the Earth's surface and are infrequently sampled, and thus have especially uncertain aerosol distributions and radiative impacts (IPCC, 2013; Hodzic et al., 2020). The NASA Atmospheric Tomography Mission (ATom) sampled the remote marine troposphere from 86°S to 82°N over four different seasons with a comprehensive suite of high-quality and carefully calibrated and operated physical and chemical aerosol instruments. It provides a unique dataset to improve our understanding of the remote atmospheric aerosols and thus refine global model predictions. A prerequisite for that purpose is to evaluate the accuracy and consistency of the ATom aerosol instruments.

The ATom physical sizing instruments have been recently described and evaluated in Williamson et al. (2018), Kupc et al. (2018), and Brock et al. (2019), while the Particle Analysis by Laser Mass Spectrometer (PALMS) chemical instrument during ATom has been described in Froyd et al. (2019). In this paper, we focus on the Aerodyne Aerosol Mass Spectrometer (AMS). AMS (Canagaratna et al., 2007) and Aerosol Chemical Speciation Monitor (ACSM, smaller, lower cost, and simpler to operate versions) (Ng et al., 2011), have been deployed extensively worldwide for ground aerosol monitoring (Jimenez et al., 2009; Crenn et al., 2015; Hu et al., 2015; Kiendler-Scharr et al., 2016; Zhang et al., 2018; ACTRiS, 2019). AMS has been deployed in most advanced atmospheric chemistry aircraft experiments worldwide (Dunlea et al., 2009; Middlebrook et al., 2012; Barth et al., 2015; Schroder et al., 2018; Garofalo et al., 2019; Hodzic et al., 2020; Mei et al., 2020; Morgan et al., 2020). The overall AMS concentration uncertainty (2σ) is normally reported as ±38% for organic aerosol (OA) and ±34% for inorganics, while the precision is typically much better, except at concentrations near the detection limit (Bahreini et al., 2009; Jimenez et al., 2016). A detailed evaluation of those uncertainties requires both very careful AMS characterization and calibration, as well as high-quality collocated measurements, as was the case in ATom.

This work uses the extensive ATom field dataset for remote aerosols to evaluate (1) the consistency of the different submicron aerosol volume measurements, (2) the quantification ability of the

64 AMS for remote aerosols, and (3) the size ranges contributing chemical composition information to

65 different instruments for ATom, and their variation with altitude. Volume comparisons probe the ability

66 of the AMS to quantify total mass and predict aerosol density based on fractional composition accurately,

67 and hence is the most germane comparison for total quantification. We examine in detail the accurate

68 quantification and application of the AMS transmission efficiency (E_L) to the particle volume

69 intercomparisons in this study. This study also serves as the basis for a future study on individual chemical

70 species intercomparisons.

2 Methods

2.1 ATom overview

73 The Atmospheric Tomography Mission (ATom) consisted of four series of flights onboard the

74 NASA DC-8 over the middle of the Pacific and Atlantic oceans, spanning from 82° N to 86° S latitude,

75 to characterize the composition and chemistry of the global background troposphere. Over two years, the

76 DC-8 aircraft was deployed once a season: July-August 2016 (ATom-1), January-February 2017 (ATom-

77 2), September-October 2017 (ATom-3), and April-May 2018 (ATom-4). During these flights, the DC-8

78 repeatedly ascended and descended between ~0.18 and ~13 km altitudes at regular intervals, typically

79 every hour (with a single vertical profile lasting ~25 min), leading to executing ~140 vertical profiles of

80 the troposphere per deployment. The unique spatio-temporal coverage and high-quality measurements of

81 this campaign ensure that its data will be used very widely, such as to evaluate and constrain global

82 modeling. Therefore it is of high interest to document the consistency of the multiple aerosol

83 measurements. This analysis is also useful to re-evaluate the quantification uncertainties of the AMS for

84 a wide range of particle concentrations and composition (e.g., Fig. S1 in the supplementary info, SI). Due

85 to the similarities in the geographic coverage of ATom studies, we focus on the intercomparisons for the

86 first two ATom campaigns in the following analysis.

2.2 Definitions of particle diameters

88 Conversions between different particle diameter definitions are required for meaningful

89 instrument comparisons. For example, particle size spectrometers report estimated geometric diameter

90   (d_p), which is derived from multiple condensation particle counters using an inversion method, or from

91   light scattering signals by using an assumed constant refractive index for aerosols. AMS transmission

92   operates in vacuum aerodynamic diameter (d_{va}) since its aerodynamic lens and supersonic expansion

93   operate in the free molecular regime (DeCarlo et al., 2004). Impactors (Marple et al., 1991, 2014) and

94   cyclones (typically sourced from URG Corp., Chapel Hill, NC, USA) are often installed upstream of

95   aerosol instruments to preselect desired aerosol ranges for ground or aircraft measurements. The cutoff

96   sizes of both devices follow the transition-regime aerodynamic diameter (d_{ta}; as the size range of interest

97   to this study is in the transition regime, requiring a "slip correction"). A detailed discussion of particle

98   diameters definitions can be found in DeCarlo et al. (2004). d_{va} is related to the volume-equivalent

99   diameter (d_{ve}, the diameter that would result if the particle was melted to form a sphere of the same density

100 as the particle and without any internal voids) as:

$$d_{va} = \frac{\rho_p}{\rho_0} \frac{d_{ve}}{\chi_v} \tag{1}$$

101 where ρ_p is the particle density, ρ_0 is the standard density (1 g cm^{-3}), and χ_v is the vacuum (i.e., free-

102 molecular regime) dynamic shape factor (=1 for spheres and >1 for non-spherical particles). Since the

103 aerosols sampled during ATom were remote and aged, we assume $\chi_v \sim 1$ and $d_{ve} \sim d_p$. The transition-

104 regime aerodynamic diameter can be calculated as:

$$d_{ta} = d_{ve} \sqrt{\frac{1}{\chi_t} \frac{\rho_p}{\rho_0} \frac{C_c(d_{ve})}{C_c(d_{ta})}} \tag{2}$$

105 where χ_t is the transition-regime dynamic shape factor, and C_c is the Cunningham slip correction factor.

106 In this study, χ_t is assumed as 1 and C_c is calculated based on air pressure. Although a given particle

107 always has the same dry d_p and d_{va}, the dry d_{ta} changes with pressure. To distinguish the d_{ta} calculated at

108 different altitudes, we use $d_{ta,sea}$ to denote that calculated at sea level ($P = 1013$ mbar) and $d_{ta,air}$ for

109 sampling aloft with an aircraft (or at an elevated ground site). In addition, all diameters change under

110 humid/dry conditions due to water uptake or evaporation (DeCarlo et al., 2004).

Atmospheric
Measurement
Techniques
Discussions

Open Access

EGU

2.3 AMS description and quantification

The highly customized University of Colorado (CU) high-resolution time-of-flight aerosol mass spectrometer (HR-ToF-AMS, hereafter referred to as AMS; Aerodyne Research Inc., Billerica, MA) (DeCarlo et al., 2006) measured non-refractory, bulk submicron particles composition at 1 Hz resolution. The AMS uses an aerodynamic lens to sample particles into a high vacuum, where they impact and vaporize on a hot porous tungsten vaporizer (600 °C). The evaporated constituents undergo electron ionization (EI), with the resulting ions being detected by a mass spectrometer (Jayne et al., 2000; Jimenez et al., 2003; Drewnick et al., 2005; DeCarlo et al., 2006; Canagaratna et al., 2007). The mass concentration of a species, s, within a multi-component aerosol particle can be calculated from the measured ion signal with the following equation (Alfarra et al., 2004; Canagaratna et al., 2007; Jimenez et al., 2016):

$$C_s = \frac{10^{12}}{CE_s} \frac{MW_{NO3}}{RIE_s IE_{NO3} Q N_A} \sum_{all\ i} I_{s,i} \tag{3}$$

where C_s is the mass concentration of species s, MW_{NO3} is the molecular weight of nitrate, CE_s is the collection efficiency of species s, RIE_s is the relative ionization efficiency of species s (to nitrate), IE_{NO3} is the ionization efficiency of nitrate, Q is the volume flow rate into the AMS, N_A is Avogadro's number, $I_{s,i}$ is the ion signal from ion i produced from species s, and the 10^{12} factor accounts for unit conversions.

CE is typically defined as the efficiency with which particles entering the AMS inlet are detected. It has been formally defined as a product of aerodynamic lens transmission efficiency for spherical particles (E_L), transmission efficiency correction for non-spherical particles (E_s) due to additional particle beam broadening, and detection efficiency at the vaporizer (E_b), which can be reduced due to particle bounce. It is thus expressed as

$$CE = E_L \times E_s \times E_b \tag{4}$$

(Huffman et al., 2005; Canagaratna et al., 2007; Middlebrook et al., 2012). Previous studies have shown that E_s~1 for ambient particles (Huffman et al., 2005; Salcedo et al., 2007), and thus CE is determined by E_L and E_b. When the mass size distribution being sampled is mostly within the region where E_L~1, then $CE \sim E_b$. Most literature papers make that implicit approximation, although it is not clear that the approximation is always justified, since E_L changes in time and between instruments and is infrequently

Atmospheric
Measurement
Techniques
Discussions
Open Access
EGU

135   quantified as it is experimentally challenging to do so. E_b depends on particle viscosity and thus phase

136   (Matthew et al., 2008; Middlebrook et al., 2012; Pajunoja et al., 2016). With the "standard vaporizer"

137   used in this study (Hu et al., 2020), ambient aerosols in continental regions typically have $E_b \sim 0.5$, but a

138   range between 0.5 to 1 can be observed (Middlebrook et al., 2012; Hu et al., 2017, 2020). E_b increases

139   for certain compositions that lead to less viscous particles, such as high ammonium nitrate mass fraction

140   or high acidity conditions, which can be estimated with a parameterization based on aerosol composition

141   (Middlebrook et al., 2012; Hu et al., 2017, 2020; Nault et al., 2018). Such parametrizations assume

142   internally mixed aerosols, which is typically the case for submicron ambient aerosol away from sources

143   due to condensation and coagulation (Petters et al., 2006; Wang et al., 2010; Mei et al., 2013). CE is

144   estimated to contribute substantially to the overall uncertainty of AMS concentration measurements

145   (Bahreini et al., 2009).

146   The main submicron inorganic ambient aerosol species are ammonium (NH_4), sulfate (SO_4),

147   nitrate (pNO_3), and chloride (Chl), and in marine areas, sea salt. The charges are omitted for the AMS-

148   measured nominally inorganic species, as the AMS may also detect some SO_4 or NO_3 signals from

149   organosulfates or organonitrates (Farmer et al., 2010). To avoid the confusion between the NO_3 radical

150   and particle NO_3, pNO_3 is used to denote total particle NO_3 explicitly (Nault et al., 2018). $RIEs$ for the

151   inorganic species can be calibrated regularly (including in the field). However, similar explicit

152   calibrations cannot be readily performed for the thousands of individual organic aerosol (OA) molecules

153   in ambient particles. Thus, laboratory-based calibrations with a limited set of OA species have been used

154   to estimate RIE_{OA} (Slowik et al., 2004; Dzepina et al., 2007; Jimenez et al., 2016; Robinson et al., 2017;

155   Xu et al., 2018), and this approach has been verified using laboratory and field intercomparisons with

156   other instruments (Takegawa et al., 2005; Dzepina et al., 2007; DeCarlo et al., 2008; Bahreini et al., 2009;

157   Dunlea et al., 2009; Timonen et al., 2010; Docherty et al., 2011; Middlebrook et al., 2012; Crenn et al.,

158   2015). Bahreini et al. (2009) estimated the uncertainty in RIE_{NH4} (which is always calibrated in the field)

159   to be ~10% vs. 15% for the other inorganics (sulfate, chloride; since most AMS users do not perform in-

160   field calibrations for those or do so less frequently). Compared to the inorganics, the uncertainty in RIE_{OA}

161   was estimated to be higher at 20%, to account for the diversity of species (Bahreini et al., 2009). An

162   average $RIE_{OA} \sim 1.4$ was determined from laboratory calibrations. However, there are conflicting reports

163 for RIE_{OA} of chemically-reduced species such as hydrocarbons, with some values around 1.4 and others

164 higher (Slowik et al., 2004; Dzepina et al., 2007; Docherty et al., 2011; Jimenez et al., 2016; Reyes-

165 Villegas et al., 2018; Xu et al., 2018). However, such species were insignificant during ATom. For more

166 oxidized species, relevant to most biomass burning OA and secondary organic aerosol (SOA), average

167 laboratory RIE_{OA} overlaps within uncertainties of 1.4 (Jimenez et al., 2016; Xu et al., 2018). Reviews on

168 this topic (Jimenez et al., 2016; Murphy, 2016a, 2016b) have emphasized the need for additional

169 investigation of AMS quantification in the field. For the AMS reported mass concentration, uncertainties

170 (i.e., accuracies) in CE (30%), RIEs (20% for OA, 15% for SO_4/Chl, and 10% for NH_4), and IE_{NO3} (10%)

171 dominate the total reported uncertainties in most situations, although precision (statistical) error becomes

172 important at low concentrations and short averaging times.

2.4 AMS operation during ATom

174   The aircraft operation of the CU AMS has been discussed previously (DeCarlo et al., 2006, 2008,

175 2010; Dunlea et al., 2009; Cubison et al., 2011; Kimmel et al., 2011; Schroder et al., 2018). The specific

176 operational procedures used during ATom have been discussed in Nault et al. (2018) and Hodzic et al.

177 (2020). Important operation details of AMS that are relevant to this study are described below. Per aircraft

178 conventions, mass concentrations are reported at $\mu g\ sm^{-3}$ (microgram per cubic meter air volume at

179 standard conditions of $T = 273.15$ K and $P = 1013$ mbar, hereafter referred to as STP. Note that many

180 definitions of STP are in use, especially in other fields).

181   Ambient aerosols were sampled through an NCAR High-Performance Instrumented Airborne

182 Platform for Environmental Research (HIAPER) Modular Inlet (HIMIL) (Stith et al., 2009) mounted on

183 a 4" raised platform on the window plate to ensure that sampling occurred consistently outside the DC-8

184 boundary layer (Vay et al., 2003). Aerosols were introduced at a constant standard flow rate of 9 sL min^{-1}

185 (up to ~9 km, 15 L min^{-1} above that; "s" refers to standard conditions, and no "s" indicates a volumetric

186 flow at in-situ T and P), with 1 L min^{-1} being continuously subsampled into a pressure controlled inlet

187 (PCI) operated at 250 mbar (187 Torr) (Bahreini et al., 2008). A fraction of that flow, 94 scm^3 min^{-1}, was

188 then sampled into the high vacuum region of the mass spectrometer through an aerodynamic focusing

189 lens operated at 2.00 mbar (1.50 Torr). Due to the much lower ambient air pressure at high altitudes, the

Atmospheric
Measurement
Techniques
Discussions

Open Access

EGU

190   PCI pressure cannot be maintained at 250 mbar above ~9 km, resulting in a drop in lens pressure (down

191   to 1.00 Torr) and flow (down to 55 scm^3 min^{-1}) at the max altitude (12.5 km). Residence times from the

192   tip of the HIMIL to the aerosol vaporizer varied from ~0.4 s in the boundary layer and ~0.9 s at 12 km

193   during ATom (Fig. S2 in SI; note that, a detailed characterization of HIMIL and PCI performance is

194   included in SI as Sect. 4 with Figs. S2-S9). The relative humidity (RH) in the line was not actively

195   controlled but was very low, on average 10 ± 21 % in ATom-1 and -2 with a median of 0.4%, due to the

196   thermal gradients between the plane cabin and ambient (T_{rack} - $T_{ambient}$ = 27 ± 13 K) (8% of the data

197   was >40% RH, including 3% >80% RH, which could increase CE). Composition-dependent CE was

198   estimated based on the Middlebrook et al. (2012) parameterization and was on average 0.87 ± 0.15 and

199   0.90 ± 0.13 for ATom-1 and -2, respectively, mainly due to high acidity (Fig. S10). After every research

200   flight, IE_{NO3} was calibrated by atomizing pure NH_4NO_3 solutions and selecting 400 nm (mobility

201   diameter, d_m; equivalent to d_{va} = 550 nm) (DeCarlo et al., 2004) particles with a differential mobility

202   analyzer (DMA, TSI model 3081, St. Paul, MN, USA) into AMS. RIEs for sulfate, ammonium, and

203   chloride were determined by multiple in-field calibrations.

204   A summary plot of the in-field calibrations of these parameters is shown as Fig. S11. Assuming a

205   constant instrument response over the course of each deployment, the variability of the calibrations can

206   be taken as an estimate of the random component of RIE uncertainty. Uncertainties (2σ) for RIE_{NH4},

207   RIE_{SO4}, and RIE_{Chl} are hence 4% (6%), 4% (2%), and 5% (8%), respectively for ATom-1 (ATom-2), all

208   smaller than the reported values from Bahreini et al. (2009). The 2σ variability of IE_{NO3} (normalized as

209   its ratio to the air beam signal, IE_{NO3}/AB) is 6% for ATom-1 and 15% for ATom-2. The propagated AMS

210   uncertainties using these values, 31% for inorganics and 37% for organics, are similar to those from

211   Bahreini et al. (2009), due to the dominant uncertainty contribution from CE (30%).

212   IE_{NO3} calibrations, performed in event trigger mode with 400 nm ammonium nitrate aerosol

213   (Schroder et al., 2018), also provided multiple AMS transmission measurements throughout the

214   campaign, by a direct comparison of the single-particle AMS counts with a Condensation Particle Counter

215   (CPC) (Nault et al., 2018). Besides this single-size (at the edge of the E_L~1 range) post-flight calibrations,

216   the upper end of the AMS transmission curve was characterized on the aircraft during ATom-2 by

217   measuring multiple sizes of monodisperse ammonium nitrate (d_m range 350-850 nm). The resulting

218   transmission accounts for all the losses in the PCI and aerodynamic lens. A calculation of the inlet line

219   losses is presented in the SI, and based on these calculations additional losses are very small and can be

220   ignored. These calculations do not include the transmission of the actual HIMIL aircraft inlet (Stith et al.,

221   2009), nor the secondary diffuser inside the HIMIL. To confirm the aircraft probe related size-dependent

222   losses or enhancements did not impact the overall transmission, the AMS sampled several times at

223   different altitudes off the University of Hawaii (UH)/NASA Langley Aerosol Research Group (LARGE)

224   inlet used by the NOAA instruments over the course of the four ATom deployments, which transmits

225   particles to ~3-5 µm $d_{ta,air}$ with 50% passing efficiency (McNaughton et al., 2007; Brock et al., 2019). No

226   difference in volume comparison (discussed in Sect. 3.2) was found under those conditions, nor in

227   previous missions with on average larger accumulation mode peaks (Fig. S4) hence we conclude that this

228   is a valid assumption.

229   Another concern for airborne sampling with an AMS is the misalignment of the aerodynamic lens

230   due to mechanical stress during flight. Such a misalignment will not necessarily be caught by the

231   previously described calibrations, since they do not probe the full surface of the vaporizer, and since lens

232   focusing can have some size-dependence. Hence for ATom 2-4, a particle beam width probe (Huffman

233   et al., 2005) was flown and profiles of both the air and particle signal were taken at most airports during

234   the mission, as shown in Fig. S9, directly confirming the lack of change in lens alignment.

235   During ATom, the AMS was operated in the fast mass spectrum mode (Kimmel et al., 2011),

236   allowing for high-time-resolution measurements at 1 Hz. For every minute, AMS started with fast mass

237   spectrum mode with the particle beam blocked (instrumental background measurement; 6 s) and then

238   with the beam open (background plus ambient air and particles; 46 s) and ended with efficient particle

239   time-of-flight (ePToF) mode (nominally 8 s), which measured speciated size distributions. The

240   interpolated average of two consecutive background signals (beam closed) was subtracted from 1 s

241   ambient signals (beam open). Also, fast blanks (20 s) were scheduled every 18 minutes by directing

242   ambient air through a high-efficiency particulate air (HEPA) filter, serving to characterize the AMS zero

243   (field background) and as a leak check downstream of the HEPA filter (Nault et al., 2018). It also serves

244   as a frequent confirmation for the real-time continuous detection limits estimated using the method

245   proposed in Drewnick et al. (2009). AMS data were reported at 1 s and 1 min time resolutions. For the 1

246 min product, the raw mass spectra were averaged prior to data reduction and analysis, which reduces

247 nonlinear spectral fitting noise for the least-squares error minimization method. This is observed because

248 a fit to the 1 min average spectrum has less fitting noise than the average of the fits to the 1 s spectra. In

249 the following analysis, the 1 min data product is used due to their improved signal-to-noise ratio (SNR).

250 Since the aerosol loadings were typically low and changed slowly in the global remote regions, longer

251 averaging times were used for some analyses. Continuous time-dependent detection limits (DLs) were

252 estimated using the method of Drewnick et al. (2009) and corrected by comparison with the periodic filter

253 blanks. The average DLs for the 1 min data were 76, 10, 6, 1, 7, 30 ng sm^{-3} during ATom-1 and 133, 18,

254 9, 2, 10, 40 ng sm^{-3} during ATom-2 for OA, SO$_4$, pNO$_3$, NH$_4$, Chl, and sea salt, respectively. Sea salt is

255 an important submicron aerosol component when sampling the marine boundary layer in ATom.

256 Although sea salt is not a standard AMS data product, in this study, we report AMS sea salt mass

257 concentrations with the method from Ovadnevaite et al., (2012) with a laboratory-calibrated response

258 factor, $9.8{\times}10^{-3}$, for the AMS sea salt marker Na^{35}Cl. Additional species were reported for ATom, with

259 DLs for MSA (methanesulfonic acid) and ChlO$_x$ (perchlorate) of 2 and 1 ng sm^{-3} during ATom-1, 3 and

260 2 ng sm^{-3} during ATom-2. Iodine and bromine were also quantified with DLs of 0.4 and 1.5 ng sm^{-3}

261 during ATom-1, 0.5 and 2 ng sm^{-3} during ATom-2, as reported by Koenig et al. (2020). The variation in

262 AMS detection limits across species is mostly controlled by differences in background signals for

263 different ions. Many of these detection limits are lower than for typical AMS aircraft operation, especially

264 during the first several hours of each flight, due to the use of a cryopump in the CU AMS (Jayne, 2004;

265 Campuzano-Jost, 2012).

266   For the purpose of instrument comparisons, we estimate the aerosol volume based on the chemical

267 instruments (V_{chem}). The contribution of the AMS to V_{chem} is determined from the AMS mass

268 concentrations by assuming volume additivity, with an average particle density estimated as (DeCarlo et

269 al., 2004; Salcedo et al., 2006):

$$\rho_m = \frac{OA + SO_4 + pNO_3 + NH_4 + Chl}{\dfrac{OA}{\rho_{OA}} + \dfrac{SO_4 + pNO_3 + NH_4}{1.75} + \dfrac{Chl}{1.52}} \tag{5}$$

270   The OA density (ρ_{OA}) is estimated with the AMS measured O/C and H/C atomic ratios of OA

271 using the parameterization of Kuwata et al. (2012) (when OA is under the detection limit and hence no

Atmospheric
Measurement
Techniques
Discussions

272   elemental ratios can be calculated, we assumed a default ρ_{OA} of 1.7 g cm^{-3} based on typical OA elemental

273   ratios found for concentrations close to the DL). The "improved-ambient" method was used for OA

274   elemental analysis (Canagaratna et al., 2015; Hu et al., 2018). The combined density of SO$_4$, NH$_4$, and

275   pNO$_3$ is assumed as 1.75 g cm^{-3}, an approximation from ammonium sulfate, ammonium bisulfate, and

276   ammonium nitrate (Sloane et al., 1991; Stein et al., 1994; Salcedo et al., 2006). The non-refractory

277   chloride density is assumed as 1.52 g cm^{-3} based on ammonium chloride (Salcedo et al., 2006). The

278   frequency distributions of ρ_m and ρ_{OA} are summarized in Fig. S12. The mass-weighted average ρ_m is

279   1.60 ± 0.14 g cm^{-3} and 1.70 ± 0.10 g cm^{-3}, and ρ_{OA} (averaged from above the concentrations above OA

280   DL) is 1.51 ± 0.19 g cm^{-3} and 1.59 ± 0.24 g cm^{-3} for ATom-1 and ATom-2, respectively. Negative AMS

281   mass concentrations exist at low concentrations since the AMS uses a difference measurement (signal

282   minus background). These negative AMS mass concentrations are kept as they are in deriving V_{chem},

283   otherwise, a positive statistical bias would be introduced if a zero or a positive value was artificially

284   assigned to those data points.

2.5 Other aerosol measurements used in this study

286   The following instruments all sampled through the LARGE inlet, except Soluble Acidic Gases

287   and Aerosol (SAGA). The transmission efficiency for this inlet has been characterized as a function of

288   particle size by flying the NASA DC-8 in a previous campaign (McNaughton et al., 2007), demonstrating

289   a unity efficiency up to supermicron size ranges and reaching 50% at $d_{ta,air}$ of ~5 µm at the surface and

290   3.2 µm at 12 km. Hereafter, we refer to the 50% transmission diameter as d_{50}.

291   *Particle size spectrometers:* Dry particle size distributions for d_p from 2.7 nm to 4.8 µm were

292   reported at 1 Hz using three optical particle spectrometers, including a Nucleation-Mode Aerosol Size

293   Spectrometer (NMASS; custom-built; 0.003-0.06 µm) (Williamson et al., 2018), an Ultra-High

294   Sensitivity Aerosol Spectrometer (UHSAS; Droplet Measurement Technologies, Longmont, CO, USA;

295   0.06-1 µm) (Kupc et al., 2018), and a Laser Aerosol Spectrometer (LAS; LAS 3340, TSI, St. Paul, MN,

296   USA; 0.12-4.8 µm), all operated by NOAA Earth System Research Laboratory (ESRL). Two NMASS,

297   two UHSAS (during ATom-2 and -3, a 300 °C thermodenuder was installed upstream of the detector of

298   the second UHSAS to volatilize refractory components), and one LAS comprise the package of Aerosol

Atmospheric
Measurement
Techniques
Discussions
Open Access
EGU

299 Microphysical Properties (AMP). Brock et al. (2019) discussed extensively the data inversion method to

300 merge the three non-thermally denuded size distributions into one. Hereafter, we refer to the non-

301 thermally denuded integrated volume (2.7 nm-4.8 µm) as the physical sizing-based volume (V_{phys}). AMP

302 performed well during ATom. Most relevant to the AMS size range, the UHSAS reported volume was

303 estimated to have an asymmetric uncertainty of +12.4%/-27.5% due to the differences in refractive index

304 (*n*) between ambient particles and assumed ammonium sulfate particles ($n = 1.527$, which is similar to

305 the refractive index found for aged ambient OA (Aldhaif et al., 2018)). This uncertainty range is estimated

306 to be between 1σ and 2σ depending on the conditions. Here we assume that it represents 1.5σ when using

307 it for uncertainty analyses.

308 ***SP2:*** Refractory Black Carbon (rBC, as defined in Petzold et al. (2013)) mass concentrations in

309 the accumulation mode size range were measured by the NOAA Single Particle Soot Photometer (SP2;

310 Droplet Measurement Technologies, Longmont, CO, USA) (Schwarz et al., 2010b; Katich et al., 2018).

311 The ATom SP2 detection system was operated as in Schwarz et al. (2010a) with a size range for rBC

312 mass of d_{ve} ~90-550 nm (Schwarz et al., 2010b). This size range typically contains ~90% of the total rBC

313 mass in the ambient accumulation mode (Schwarz et al., 2008; Shiraiwa et al., 2008).

314 ***PALMS:*** The Particle Analysis by Laser Mass Spectrometry (PALMS) is a single-particle laser-

315 ablation/ionization mass spectrometer instrument that measures size-resolved ($d_p \sim 0.1$-5 µm) particle

316 chemical composition with fast response (Thomson et al., 2000; Murphy et al., 2006). Particle mass

317 concentrations can be derived as a function of size when mapping the PALMS chemical composition to

318 the size distributions reported from the UHSAS and LAS, which is referred to as the PALMS-AMP

319 products (Froyd et al., 2019). In this study, we focus on the different particle size ranges observed by

320 PALMS and AMS, to illustrate the strengths and applications of the two aerosol composition instruments

321 onboard the DC-8.

322 PALMS is the most complex of the chemical composition instruments used in ATom. It is a single-

323 particle based instrument with both a very steep detection efficiency vs. particle size in the smaller particle

324 range and the ability to measure much larger particles than the AMS. While the total reported mass (with

325 some density uncertainty) of the PALMS-AMP products will always match the physical volume

326 measurement over the range that PALMS reports (100-5000 nm d_p), the uneven sampling data coverage

327 of particles across each size bin, as well as the broadness of the bins chosen for PALMS-AMP analysis,

328 can lead to a chemical bias if composition gradients exist within a bin (Fig. S13). Therefore, care must be

329 taken to balance statistical representativeness against the need for unvarying particle composition across

330 the size range over which those statistics are obtained (Froyd et al., 2019).

331 For intercomparisons we characterize the specific size range over which the PALMS can obtain

332 sufficient chemical information over a given time period under the ATom conditions, which is mainly

333 limited by particle statistics. If zero or a very low number of particles is sampled for a given AMP size

334 bin and time period, there is no real information being captured for characterizing the composition of the

335 particles in that bin. That is true even if the AMP volume in that bin is assigned a composition by

336 extrapolating the composition of larger or smaller particles. Therefore, we derived the PALMS detected

337 particle numbers based on the raw AMP size resolution (20 bins/decade, 34 bins in total above 100 nm d_p

338 for the size range that PALMS-AMP reports) to avoid the assumption of homogeneous chemical

339 composition within four broader bins in Froyd et al. (2019). This provides an alternative illustration of

340 PALMS size coverage and introduces a method that is applicable to other single-particle mass

341 spectrometers or other particle-counting based chemical instruments. A sensitivity test was carried out at

342 various size resolutions, shown as Fig. S14, with more detected particles per bin for larger bins, as

343 expected. Importantly, the 20 bins/decade size resolution of AMP is preferable as it makes the results

344 directly comparable to the other aerosol instruments. The probability of detecting on average one valid

345 particle per AMP size bin in the PALMS is very low below ~160 nm and above 1000 nm over a typical

346 3 min analysis period (Fig. S14). As altitude increases in the free troposphere, the size distribution often

347 shifts to smaller diameters (Williamson et al., 2019), thus we expand the 1D profile in Fig. S14 to include

348 the altitude dependence (Fig. S15). The results are shown at 3 min, 60 min intervals, as well as campaign-

349 wide, since the 3 min timescale is most relevant for high time resolution airborne analyses while the

350 longer ones are relevant to averages by altitude in a latitude band and similar analyses that group data

351 together from different time periods.

352 Based on Froyd et al. (2019), we assume that if PALMS detects N = 1 particle in a given AMP

353 size bin, the composition of the bin is fully characterized. This particle number corresponds to N = 5

354 particles for 4 bins/decade, which is a reasonable number for the particle composition to be reasonably

Atmospheric
Measurement
Techniques
Discussions

represented by the particles captured, with a resolution over which composition changes may happen in the real atmosphere (Zhang et al., 2004). For simplicity, we scale the fraction of the particles contributing information content linearly for conditions with N < 1.

SAGA: gas-phase HNO_3 plus particulate inorganic nitrate, and sulfate were measured online with the University of New Hampshire (UNH) SAGA mist chamber (MC) ion chromatography (IC) at a time resolution of ~80 s. Water-soluble chemical species were also measured offline by collecting particles with Zefluor filters (9 cm diameter, 1 mm thick, and 1 µm pore size, from MilliporeSigma Corp., Burlington, MA, USA) with subsequent procedures as described by Dibb et al. (1999, 2000) and Heim et al. (2020). In brief, filter samples were collected during level portions of each flight, stored over dry ice, extracted with ultrapure water, and sent back to the lab in UNH for IC analysis to quantify more species than the MC (Dibb, 2019).

SAGA filters were sampled from the UNH inlet with an estimated cutoff size of 4.1 µm ($d_{ta,sea,50}$) at the surface and 2.6 µm ($d_{ta,air,50}$) at 12 km (McNaughton et al., 2007). The SAGA MC sampled from a glass-coated (vapor deposited) manifold (8 cm inner diameter) with high airflow (on the order of 2000 sL m^{-3} at low altitude) (as shown in Fig. S16). The diffuser type configuration at the manifold entrance boosts airflow and the surrounding piece at the pipe tip excludes cloud droplets and giant sea salt particles (Talbot et al., 2003). The in-cabin part of the pipe till MC was heated to 50 °C to minimize HNO_3 wall deposition, although sampled air T is assumed to be the same as ambient due to the high airflow and short residence time (~0.2 s). A small glass tube from MC, which is sealed at the bottom and opens a small hole on the downstream side, sticks down into the manifold. This configuration provides a particle cutoff size of ~1µm ($d_{ta,sea,50}$) at the surface and lower at higher altitudes (van Donkelaar et al., 2008).

To be compared with other ATom aerosol measurements, the pressure-dependent SAGA MC and filter inlet transmissions are calculated based on the ATom conditions and summarized in the SI as Fig. S17 and S18, respectively.

Use of data from other instruments for V_{chem}: V_{phys} includes refractory species, such as rBC, sea salt, and dust, and thus their volumes need to be added to the AMS non-refractory volume before comparison. rBC volume is estimated from SP2 mass measurements (Katich et al., 2018) with a density of 1.77 g cm^{-3} (Park et al., 2004). The sea salt volume is estimated from its AMS mass concentration with

Atmospheric
Measurement
Techniques
Discussions
Open Access
EGU

383 a density of 1.45 g cm^{-3}, assuming particles had not fully effloresced prior to detection (Froyd et al.,

384 2019). Sea salt is typically externally mixed with sulfate-organic-nitrate particles (Froyd et al., 2019),

385 therefore, it is not routinely considered in the AMS aerosol density estimation (i.e., in Eq. 5). The

386 exclusion of dust in the volume closure is reasonable in general based on the results in Sect. 3.2 due to

387 the limited impacts from dust for ATom, on average 1.1 ± 4.3 % (median = 0.0 %) of the AMS observed

388 volume, but it can contribute as high as 95% for occasional short plumes encountered in ATom-2 (Fig.

389 S19) (Froyd et al., 2019). Besides, we exclude the last ATom-1 research flight (a transit flight in the

390 continental U.S. from Minneapolis, MN to Palmdale, CA, different from the remote marine atmosphere

391 of the other ATom flights) and <10 min of sampling impacted by volcanic ash near Hawaii in ATom-2

392 (Research Flight 203, Jan 30, 2017). As discussed above, we use 1-min AMS data for intercomparison,

393 and 1 s V_{phys} is averaged to the same time scale. There may be a minor bias introduced from this approach

394 since AMS periodic blank measurements exclude some 1-sec data points from the AMS but not from

395 V_{phys} (~3% of the total 1-sec V_{phys} points), and similarly, some data are removed from the sizing

396 measurements due to cloud masking but not for the AMS (13%, discussed below in Sect. 3.2). In this

397 study, the particle volume is reported in units of μm^3 scm^{-3}, where scm^{-3} are cubic centimeters of air under

398 STP.

2.6 Summary of the ATom aerosol size distribution and instrument size ranges

400 Fig. 1 summarizes the ATom-2 campaign averaged number and volume size distributions from

401 AMP and compares it to the subranges observed from several ATom aerosol instruments, to provide

402 context for this study and future instrument comparisons based on the ATom dataset. The upper cut sizes

403 for LAS, SAGA MC, and filter, determined from their inlets, move towards smaller particles at higher

404 altitudes, thus the size ranges plotted in Fig. 1 for these instruments are the best-case scenario (in the

405 planetary boundary layer). In contrast, the AMS transmission stays the same up to ~9 km. Based on Fig.

406 1, the AMS size range is more closely comparable to SAGA MC, and comparison to all the other

407 instruments requires considering the different size ranges. Therefore, accurately characterizing AMS

408 transmission is a prerequisite for quantitative instrumental intercomparisons. While the focus of this work

409 is on instrument comparisons, we want to emphasize that a properly characterized size cut is also

Atmospheric
Measurement
Techniques
Discussions

Open Access

EGU

410   important for model comparisons and that the size bins used in most global models, typically reported as

411   d_p, vary widely (Hodzic et al., 2020).

3 Results and Discussion

3.1 AMS transmission

414   AMP gives nearly unity detection efficiency of the particles (not lost in the inlet) from ~5 nm to

415   ~4 µm (d_p) at sea level, and 50% transmission at 2.7 nm and 4.8 µm (inlet-limited), of which AMS, SAGA

416   MC, PALMS, and SP2 observe a subrange, as shown in Fig. 1 (McNaughton et al., 2007; Brock et al.,

417   2019). Therefore, the volume derived from the AMP size distributions (V_{phys}) can be used as the basis for

418   intercomparisons. Characterizing AMS transmission (E_L) is critical for a meaningful comparison of V_{phys}

419   vs. V_{chem}.

420   AMS transmission (always specified vs. d_{va}) can be quite variable between instruments, and can

421   also change for a specific AMS in time, so it is critical to characterize the transmission in the field for

422   meaningful instrumental intercomparisons (Liu et al., 2007; Knote et al., 2011; Hu et al., 2017; Nault et

423   al., 2018). During ATom, the large particle region (~500-1200 nm, d_{va}) of the CU AMS transmission was

424   calibrated in the field (Fig. 2), as discussed in Sect. 2.4. A fit to the multi-size field calibrations indicates

425   a 100% transmission at d_{va} of ~483 nm (1σ range: 445-525 nm) and a 0% transmission at ~1175 nm

426   (1112-1241 nm), with 50% transmission at 754 nm. This transmission was stable throughout the ATom-

427   1 and -2 deployments. Other than new particle formation and growth events, the small particle end of the

428   transmission curve is less critical in determining submicron aerosol volume since volume is normally

429   dominated by the accumulation mode (which normally refers to the range 100-1000 nm d_{ta}) (Seinfeld and

430   Pandis, 2016) instead of the Aitken mode (10-100 nm d_{ta}). Brock et al. (2019) found the accumulation

431   mode during ATom to be 60-500 nm d_p, equivalent to 93-674 nm in $d_{ta,sea}$, as remote particles were far

432   away from sources of precursor gases that could sustain growth to larger sizes. Results from previous

433   measurements (Zhang et al., 2004; Knote et al., 2011) were used to estimate the small particle

434   transmission, with 0% at 35 nm and 100% at 100 nm. Sensitivity tests on the small particle transmission

435   points (Sect. 3.3 below) confirm a lack of impact on the volume comparison for ATom conditions. AMS

436   transmission curves for all ATom campaigns are shown in Fig. 3. Importantly, AMS transmission

437   improved noticeably for ATom-4 compared to the prior ATom legs, possibly due to small changes in the

438   inlet during reassembly. This shows the importance of characterizing E_L for each campaign for

439   quantitative intercomparisons. Similar changes have been observed in the past for other aircraft and

440   ground campaigns.

3.2 Comparison of AMS vs. standard PM$_1$ size cuts

442   AMS is often described as an approximate "PM$_1$" or "submicron" instrument. Since the standard

443   definition of PM$_1$ is based on devices that impose an aerodynamic diameter (d_{ta}) cut under ground-level

444   pressure, temperature (e.g., defined at $T = 293.15$ K and $P = 1013$ mbar (Marple et al., 1991)), and

445   humidity, the equivalent AMS transmission in d_{ta} depends on particle density and composition, as well

446   as the E_L of the specific AMS for a given study. The careful transmission calibrations and extensive

447   sampling of ATom allow more precise characterization of this cutoff size for the CU aircraft AMS and

448   remote aerosols.

449   For aircraft sampling where a submicron cut is desired (not including the AMS), the single 1 μm

450   stage from a micro-orifice uniform deposit impactor (MOUDI) (Marple et al., 1991, 2014) is often used

451   (e.g., (Peltier et al., 2008; Brock et al., 2011; Guo et al., 2016)) to preselect submicron particles

452   (transmission shown in Fig. S20). Here, we choose MOUDI instead of SAGA MC, also known as a

453   submicron cut instrument deployed for aircraft studies, due to the lack of a published transmission curve

454   for SAGA MC. Due to the higher temperature in cabin vs. ambient air (Guo et al., 2016), the MOUDI

455   impactor (operating at cabin T and ambient P) is expected to size-select dry particles, similar to the AMS.

456   The impactor provides a nominal PM$_1$ cut at $T = 293.15$ K and $P = 1013$ mbar but the $d_{ta,50}$ for a given

457   particle is pressure- and temperature-dependent, and thus varies with altitude. For instance, at an aerosol

458   density of 1.7 g cm^{-3} (the ATom-2 campaign average), $d_{ta,air,50}$ drops from 1 μm to 912 nm at 6 km, and

459   to 686 nm at 12 km height, based on the U.S. standard atmosphere (NOAA, NASA, U. S. Air Force,

460   1976), as shown in Fig. 3. Even lower cut sizes, 752 nm at 6 km and 400 nm at 12 km, are expected if the

461   impactor was operated under ambient T (not typically done, and best avoided for an optimal particle cut;

462   summarized in Table S1). Hence, the deviation from the nominal 1 μm cut size can be very significant at

463 high altitude (although it could in principle be modulated by changing the flow rate vs. altitude). The

464 pressure-dependent diffusion loss of small particles for MOUDI is estimated using the inlet system

465 onboard NCAR/NSF C-130 from Guo et al. (2016), a ~2.5 m tubing with an inner diameter of ~1.1 cm.

466 Given a flow rate of 30 L m^{-3}, Reynolds number is 3858 at sea level and increases with altitude, indicating

467 a turbulent flow in the inlet.

468   If we compare the AMS transmission to ground-level based dry d_{ta} (using a dry particle density

469 of 1.7 g cm^{-3} to calculate d_{ta} from d_{va}), the ATom-2 / 3 / 4 $d_{ta,sea,50}$ are 599 nm, 615 nm, and 758 nm,

470 respectively (the $d_{ta,air,50}$ are higher and listed in Table S1; for example, $d_{ta,air,50}$ is 782 nm and 837 nm at

471 6 km and 12km, respectively for ATom-4). Thus the cutoff size of the AMS in ATom is more stringent

472 than a MOUDI nominal PM$_1$ cut at the surface and 6 km, and less stringent at the higher altitudes in

473 ATom-4. Importantly, the AMS transmission stays constant up to ~ 9 km in altitude for the implemented

474 PCI. No in-field characterization of the AMS transmission at higher altitudes (when inlet pressure slips)

475 was performed, but laboratory calibration shows no change in transmission at 710 nm d_{va} at the max

476 altitude inlet pressure (1.05 Torr).

477   For ground studies, URG PM$_1$ standard cut (model: URG-2000-30EHB) and sharp cut (model:

478 SCC 2.229) cyclones are widely used for non-AMS instruments. The estimated diffusion loss of small

479 particles in the URG cyclones was negligible (e.g., 5% loss at $d_{ta,sea}$ = 5 nm and less loss expected at

480 larger sizes), calculated with a nominal flow rate of 16.7 L m^{-3} and assumed cyclone internal dimensions,

481 0.50 inch (1.27 cm) in diameter and 50 cm in length (Reynolds number = 2100, indicating a likely

482 turbulent flow). The two cyclones offer cutoff sizes at 1 μm at T = 293.15 K and P = 1013 mbar (Fig.

483 S20), and smaller cuts when such cyclones are deployed at lower ambient pressure and the nominal

484 volumetric flow, e.g., at a mountain site.

485   One additional complexity arises since the standard PM$_1$ cut made with URG cyclones are under

486 ambient humidity conditions (i.e., particles are not dried prior to sampling). Thus, the equivalent dry

487 particle cut size is below 1μm at sea level and depends on the amount of liquid water associated with the

488 particles. For the ATom conditions, particle size shrinks on average ~20% (assuming a complete loss of

489 the predicted particle liquid water content from the higher ambient RH, mean/median(±SD) =

490 40/36(±29)% to the lower inlet RH, 10/0.4/(±21)%; Fig. S1c-d) and the frequency distribution plots are

491 shown as Fig. S21 (SD stands for standard deviation). While AMS transmission is characterized with dry

492 particles, a smaller difference between the AMS transmissions and the cyclone transmissions is expected,

493 compared to Fig. 3. Taking the estimated ~20% shrinkage in particle size from drying in the sample line

494 (for the ATom-1 and -2 conditions), the AMS transmission would be equivalent to a standard $PM_{0.75}$ and

495 a $PM_{0.95}$ cut during ATom-2 and -4 respectively in terms of ambient aerosol size.

496 Since aerosol density affects the conversion between d_{va} and d_{ta} (Eqs. 1-2), a higher AMS $d_{ta,50}$ is

497 expected if sampling aerosols with lower densities than the ATom-2 campaign average of 1.70 g cm^{-3}. To

498 illustrate this point further, results based on an assumed 0.9 g cm^{-3} aerosol density, typical of hydrocarbon-

499 like OA from lubricating oil or oleic acid as cooking aerosol surrogate (Kuwata et al., 2012; Herring et

500 al., 2015), are shown in SI as Fig. S22b. In this case, the ATom-2 and ATom-4 AMS $d_{ta,sea,50}$ increase to

501 789 nm and 1006 nm, respectively, making the ATom-4 AMS a dry PM_1 cut when performing

502 experiments with those aerosols.

503 It is also useful to compare the sharpness of the different transmission curves. The sharpness of

504 transmission is commonly defined as $(d_{ta,16}/d_{ta,84})^{0.5}$, where $d_{ta,16}$ and $d_{ta,84}$ are particle aerodynamic

505 diameters at 84% and 16% transmissions (Peters et al., 2001). The sharpness of the AMS transmission

506 profiles are similar to that of a URG PM_1 standard cut cyclone; 1.34 in ATom-2 and 1.49 in ATom-4

507 compared to 1.35 and 1.17 of the URG standard cut and sharp cut cyclones (a lower number indicates a

508 sharper cut). The MOUDI 1μm stage impactor provides the sharpest cut at 1.12 at sea level but the

509 sharpness decreases at higher altitudes, 1.15 at 6 km and 1.22 at 12 km.

510 Including all effects, the CU aircraft AMS was approximately equivalent to a standard ground-

511 level $PM_{0.75}$ instrument during ATom-2 and a $PM_{0.95}$ instrument during ATom-4. For laboratory or field

512 experiments with oily particles with an aerosol density of 0.9 g cm^{-3}, the same AMS would be a $PM_{0.79}$

513 or $PM_{1.0}$ instrument in terms of dry aerosol size.

3.3 Volume closure

515 AMS observes a fraction of V_{phys} (Figs. 1 & 3). AMS transmission vs. d_p was calculated based on

516 the calibrated transmission vs. d_{va} (Eq. 1) and the AMS estimated time-dependent ρ_m (Eq. 5), and applied

517 to the AMP size distributions used to derive V_{phys}. This volume is referred to as $V_{phys,TC}$ (the AMS-

518   transmission-corrected V_{phys}). The comparisons between $V_{phys,TC}$ and V_{chem} for ATom-1 and -2 are shown

519   in Fig. 4. Good agreement is observed, with the data points distributed around the 1:1 line over a three

520   order-of-magnitude range of concentrations. For ATom-1 the regression slope is 0.96 and r^2 is 0.95. The

521   larger volume concentrations were generally detected in the boundary layer. Time averaging reduces

522   random noise (more dominant at smaller volumes), as evidenced when comparing this analysis for 1, 5,

523   and 10 min averages (Fig. S23). The slightly worse fitting slope of 1.09 and r^2 of 0.93 in ATom-2 may be

524   due to the larger contribution of sea salt in ATom-2 in the boundary layer (Hodzic et al., 2020) and hence

525   the larger uncertainty in applying the AMS size cut. To illustrate the impacts of sea salt, we replotted the

526   comparisons (Fig. 4a-b) colored by sea salt shown as Fig. S24a-b, which suggests that some outliers in

527   ATom-2 are observed at high sea salt concentrations. We also investigate the potential differences in the

528   data products due to the differences in raw data processing criteria for cloud artifacts between AMS and

529   NOAA size spectrometers and find no clear evidence (Fig. S24c-d). Furthermore, we confirm that

530   excluding submicron dust volume is reasonable; only a few outliers have noticeably higher contributions

531   from dust (Fig. S24e-f).

532   Species density is used to convert the AMS mass to volume concentrations and thus affects the

533   volume comparison. As discussed above (Fig. S12), ρ_{OA} in this study is estimated with the

534   parameterization method of Kuwata et al. (2012). The ρ_{OA} parameterization method from Kuwata et al.,

535   (2012) was validated up to 1.9 g cm^{-3} (i.e., oxalic acid) and the lab generated SOA in that study had up to

536   1.46 g cm^{-3} ρ_{OA} with an O/C of 0.72. The estimated ATom-1 and -2 ρ_{OA} is close to that of succinic acid,

537   1.57 g cm^{-3}, that has a similar O/C ratio (ATom-1 and -2 vs. succinic acid: 1.05 ± 0.44 vs. 1.0), and falls

538   into the observed ρ_{OA} density range, 1.5-1.7 g cm^{-3}, for low mass concentrations of SOA (< 3 μg m^{-3}, as

539   the most cases in ATom), made from α-pinene and ozone from a chamber study (Shilling et al., 2009).

540   However, ρ_{OA} estimated from PALMS, 1.35-1.45 g cm^{-3} (Froyd et al., 2019), is ~0.2 g cm^{-3} lower than

541   that estimated from AMS, for reasons that are not yet understood. As a sensitivity check, we recalculate

542   V_{chem} by subtracting 0.2 g cm^{-3} from the AMS estimated ρ_{OA} (Fig. S25). Compared to the base cases (Fig.

543   4a-b), the r^2 values barely change and the slopes increase by 5% or 8% due to the higher estimated OA

544   volume in V_{chem}. Therefore, this uncertainty is below 10% and does not undermine the agreement within

545   the uncertainties between V_{chem} and $V_{phys,TC}$.

546   To illustrate that applying the AMS transmission to V_{phys} is a prerequisite for a meaningful

547   comparison, Fig. 4c illustrates the volume closure for a research flight in ATom-2 (RF208, Feb 15 2017,

548   from Ascension to the Azores), in which the contribution of supermicron particles to total volume is

549   significant. Although V_{phys} was, in general, several times larger than V_{chem} when the DC-8 flew at lower

550   altitudes (below ~3 km), $V_{phys,TC}$ agrees very well with V_{chem}, with a regression slope of 1.04 and an r^2 of

551   0.97. To examine if applying the AMS transmission introduces a systematic bias, Fig. 4a-b was replotted,

552   colored by the removed fraction of V_{phys}, in SI as Fig. S26. The binned data points at 20% intervals show

553   little difference, suggesting that no significant bias is arising for this reason for both ATom-1 and -2. An

554   exception is the 80-100% bin for ATom-2 due to some outliers with high sea salt as shown in Fig. S26b

555   and possibly the increased statistical noise, with only 25% of the data points in this bin compared to

556   ATom-1.

557   Box plots, regressions, and correlations were carried out for the separate datasets in each bin of

558   removed V_{phys}, as shown in Fig. 5a-c. For the combined ATom-1 and -2 data (Fig. 5a), the majority of the

559   volume ratios are distributed around the 1:1 line and within the combined systematic uncertainty range

560   (combined 2σ of AMS and UHSAS, the size spectrometer that overlaps most with the AMS, see Fig. 1).

561   If using the UHSAS data product alone and applying the AMS transmission, the resulting volume is on

562   average 93 ± 9 % in ATom-1 and 87 ± 14 % in ATom-2 compared to $V_{phys,TC}$. Therefore, the UHSAS

563   uncertainty is representative of that of $V_{phys,TC}$. The V_{phys} uncertainty depends on particle size range or

564   mode (see Table 1 in Brock et al., (2019)) and the random uncertainty in V_{phys} is expected to be smoothed

565   out with longer averaging time scales. All five bins show high correlations with r^2 of 0.79-0.96, with a

566   lower correlation at the 80-100% V_{phys} removal bin. The smallest slope of 0.84 is also seen at this bin,

567   where the largest discrepancy is expected due to the combined sharpness of the decreasing AMS

568   transmission for larger particles and the rising tail of coarse mode particles into the submicron size range

569   (e.g., the AMS transmission excludes on average 89% of the total sea salt volume sampled during ATom-

570   2). When investigating ATom-1 and ATom-2 independently, ATom-1 averages are slightly below unity

571   but consistent throughout the five bins (Fig. 5b), and ATom-2 shows an increasing bias above 60% V_{phys}

572   removal (again likely due to the much higher sea salt fractional contribution for this campaign). Only the

573   80-100% bin in ATom-2 has substantial data outside the 2σ uncertainty range. Overall, the above results

21

574   suggest the in-field characterized AMS transmission is robust for the various conditions encountered in

575   the ATom-1 and -2 studies.

576   While binning the data is useful for exploring possible systematic biases, looking at the overall

577   deviations of the individual measurements allows us to explore to what extent the reported instrument

578   uncertainties are consistent with the ATom dataset. Fig. 5d-i shows the frequency distributions of the

579   volume ratio, V_{chem} / $V_{phys,TC}$, together with the combined 2σ accuracy of AMS and UHSAS. The ATom-

580   2 data distribution is slightly broader than ATom-1 partly owing to the larger precision error (e.g., when

581   mass concentration is within three times of DLs) associated with the lower submicron mass

582   concentrations, 0.38 vs. 0.50 µg m^{-3}. Longer averaging time can deemphasize the precision errors,

583   especially for a dataset like ATom with few sharp plumes. Thus we plot the volume ratio at three time

584   scales, 1 min, 5 min, and 10 min. It shows a clear improvement in the spread of the ratio as the averaging

585   time scale increases, with the 10 min data being consistent with the reported accuracies. This supports

586   the good quality and consistency of the ATom aerosol dataset, and it also supports the reported AMS

587   accuracies.

3.4 Sensitivity tests to AMS transmission

589   The above discussion demonstrates the critical role of well-characterized AMS transmission for

590   meaningful volume intercomparison. In this section, we aim to quantify the impact of the AMS

591   transmission on the volume comparison by artificially adjusting the transmission with a series of

592   sensitivity tests. As shown in Fig. 6a, the AMS transmission can be characterized by four "anchoring"

593   particle sizes, representing 0% and 100% transmissions at both ends. During ATom-1 and -2, these

594   anchoring sizes (in d_{va}) were estimated as (i) 35 nm, (ii) 100 nm, (iii) 482 nm, and (iv) 1175 nm,

595   respectively, as discussed above (Fig. 2). Uncertainty ranges are estimated for the latter two sizes from

596   the ATom calibrations and shown in Fig. 6d-e. We alter one anchoring size at a time, recalculate $V_{phys,TC}$,

597   and re-compare to V_{chem}, which is kept unchanged. The resulting slopes and r^2 are summarized in Fig. 6.

598   The adjustments at the two lower anchoring sizes, up to ± 25 nm at 35 nm and ± 50 nm at 100 nm, have

599   a negligible impact on the volume comparison due to the small volume/mass concentrations at these sizes

600   during ATom (e.g., Fig. 3), except for the unrealistic 50 nm decrease at 100 nm (the second anchoring

601 point). In contrast, a dependency of the fitting results on the details of the AMS transmission curve for

602 large particles is observed. For the third anchoring point, corresponding to the largest particles with 100%

603 transmission (Fig. 6d), a smaller d_{va} excludes more V_{phys} and results in a higher slope. For example, at the

604 lower one SD limit d_{va} of 445 nm, the fitting slopes increase from 0.97 to 1.01 for ATom-1 and 1.09 to

605 1.12 for ATom-2. These small changes in slope are the largest among the four anchoring points, and they

606 are statistically significant because the changes are one magnitude higher than the fitting 1σ uncertainties

607 of the slopes (~0.03 vs. ~0.004). In all the cases investigated, r^2 barely changes.

608 It is also of interest to compare the results if we had assumed that AMS literature transmission

609 curves applied to this study. Here we test the commonly used transmission curves of Liu et al., (2007)

610 and Hu et al., (2017). The four anchoring sizes, all in nm, in Liu et al., (2007) (Hu et al., (2017) in

611 parentheses) are (i) 50 (40), (ii) 150 (100), (iii) 300 (500), and (iv) 1400 (1500, estimated by fitting). The

612 regression slopes with the Liu curve (the Hu curve) are 1.18 and 1.23 (0.94 and 0.96) in ATom-1 and -2,

613 respectively, compared to 0.96 and 1.09 derived from applying the ATom-1 and -2 transmission (Fig. 4).

614 In summary, the above results suggest: (1) The volume closure is relatively insensitive to the uncertainties

615 of the AMS transmission curve characterized in this study; (2) Use of transmission curves from the

616 literature for uncharacterized instruments can result in substantial deviations (which may then be

617 incorrectly attributed to changes in *CE* or *RIE*); (3) The large particle region of the AMS transmission

618 curve is more important than the small particle region for ATom-1 and -2; and (4) The point (iii) with

619 100% transmission size for large particles (482 nm in this case) is the most important calibration, due to

620 the dominance of the accumulation mode mass for the submicron size range.

3.5 Characterization of the AMS observable particle fraction during ATom vs. the standard ground-based and aircraft-based PM$_1$ definition

623 It is of interest to compare the fraction of the volume detected by the AMS for ATom vs. what a

624 standard ground-level PM$_1$ (the most common definition of "submicron") instrument would detect. In this

625 study, we use the standard cut URG cyclone operating at the surface ambient humidity as the reference,

626 simulating its operation at ground sites at different altitudes (e.g., sea level and mountain sites). As

627 discussed above, both the AMS and the AMP size distributions measure dry particles while the "standard"

628 PM$_1$ is defined with practical size-selection under ambient humidity. To account for the difference, the

23

Atmospheric
Measurement
Techniques
Discussions

629 URG transmission is applied to the estimated ambient particle size before losing liquid water content (the

630 effect of water on ρ_p is also considered) (DeCarlo et al., 2004). We assume no size dependence for ρ_p or

631 the volume fraction of liquid water content for the submicron aerosols. Ambient P and T from ATom are

632 applied to the URG transmission to account for the shift at non-STP conditions, which is relevant when

633 operating such a cyclone at higher altitudes e.g., a mountain site. The results of applying the AMS and

634 URG PM_1 standard cut cyclone transmissions to V_{phys} are shown in Fig. 7. AMS observed on average 96

635 $\pm$ 16% (median 96%) and 94 $\pm$ 12% (median 94%) of the volumes that would transmit through a ground-

636 level URG PM_1 cyclone in ATom-1 and -2, respectively. Although we previously concluded that the

637 AMS was approximately an equivalent ground-level $PM_{0.75}$ instrument in ATom-1 and -2, the difference

638 in collected volume is only ~5%. This is because the submicron volume size distribution peaked around

639 300 nm (d_{ta}; see Fig. 3 for example), where AMS transmission is ~100%, and also due to the effect of

640 liquid water on particle size.

641 Next, we compared the submicron volumes observed from the CU AMS and a MOUDI 1 µm

642 stage impactor during aircraft studies, using the ATom conditions (Fig. 7c & 7d). The two inlets size-

643 select dry particles due to sample line heating. AMS observed 87% and 83% by means, 90% and 85% by

644 medians, in ATom-1 and -2 of that from an airborne MOUDI impactor, lower than the ratios when

645 comparing to the URG PM_1 cyclones for two reasons: the smaller cutoff size of URG vs. MOUDI due to

646 particle water and lower operating T for URG (which relates to air viscosity). We also compared the

647 $V_{phys,TC}$ to the (total) V_{phys} (Fig. 7a & 7b). AMS collected 68% by means (the same for ATom-1 and -2,

648 and 78% in ATom-1 and 71% in ATom-2 by medians) of V_{phys}; in other words, 32% of V_{phys} was excluded

649 by applying the AMS transmission. For both ATom-1 and -2, there was considerable variability on the

650 fraction of V_{phys} removed to obtain $V_{phys,TC}$, which spanned the range from 0% to 100% removal, thus

651 providing a good scenario of testing the AMS transmission. Nevertheless, this data shows that on average

652 the AMS captured the submicron range well, as shown in Fig. 4, and that the comparisons presented here

653 are meaningful for a wide range of scenarios.

Atmospheric
Measurement
Techniques
Discussions

Open Access

3.6 Characterization of the observable particle populations for different chemical instruments

The different parts of the aerosol population included in different measurements and models make comparisons of aerosol species inherently more complex than for gas-phase species. In this section, we characterize the size ranges that contribute information to each composition measurement. Importantly, only the particle ranges are illustrated, irrespective of the properties of each chemical detector (e.g., species measured, detection limits, etc.). Speciated particle mass concentrations can be derived by sampling the bulk aerosol using a size cut. For example, MOUDI 1 µm stage impactor and SAGA MC are suitable for size-selecting submicron range (Fig. S17). With a wider coverage expanding to supermicron sizes, SAGA filters measure up to $d_{ta,sea}$ of 4.1 µm and their estimated altitude-dependent transmissions for the ATom conditions are shown in Fig. S18. Speciated mass concentrations can also be derived as a function of size by mapping the PALMS single-particle chemical composition onto an independent physical size distribution measurement (in case of ATom the AMP size distribution products described in Brock et al. (2019)) (Froyd et al., 2019), and PALMS-AMP derived sulfate and organic mass concentrations have recently been reported to the NASA ATom archive (Wofsy et al., 2018).

Fig. 8 summarizes the approximate fractions of the volume and number distributions that each ATom instrument observed for ATom-2 (Fig. S28 shows ATom-1). A MOUDI 1 µm stage impactor is also included for comparison. SAGA filters collect nearly the entire total volume. The vertical profiles of volume size distributions collected by AMS and MOUDI are similar and converge at higher altitudes due to the shift in the MOUDI cutoff size. Both AMS and PALMS capture the accumulation mode, which often dominates particle mass, and thus agreement of the reported submicron concentrations should be expected under such conditions. The AMS samples contain chemical information about smaller particles that are typically absent from the PALMS data (Williamson et al., 2019). Conversely, the PALMS samples a significant fraction of the supermicron mode beyond the transmission range of the AMS. The PALMS-AMP at the reported AMP size resolution and 3 min time resolution is shown in Fig. 8 (and Fig S28), and similar plots for other size and time resolutions are shown in Fig. S29 and S30. 3 min corresponds to ~36 km horizontal distances and ~1.5 km vertical distances during ATom profiles and thus is a reasonable basis for comparison.

Atmospheric
Measurement
Techniques
Discussions

681   It is also of interest to quantify what fraction of the particle number is represented by each

682   instrument's data. For instance, the composition relevant to calculations of cloud condensation nuclei

683   (CCN) number concentrations would be dominated by small particles. The number fractions have

684   somewhat different meanings for the instruments. PALMS, when merged with size distribution

685   measurements, can quantify the number of particles of various types as a function of size. For the other

686   (bulk) instruments, the number fraction merely represents the number of particles in the size range where

687   mass is measured. Unlike the volume case, where the size distribution is dominated by the accumulation

688   and coarse modes, the number size distribution in ATom was dominated by the nucleation and Aitken

689   mode particles. In ATom-1 and -2, the SAGA filters, MOUDI, AMS, and PALMS-AMP (based on AMP

690   size resolution and 3 min time resolution) characterize the chemical composition on average of 96%

691   (median 99.9%), 78% (87%), 68% (74%), and 54% (55%) of V_{phys} (total AMP particle volume), and 98%

692   (99%), 89% (93%), 41% (41%), and 5% (1%) of the total AMP particle number, respectively. The size

693   range above d_p = 100 nm, for which PALMS-AMP (Froyd et al., 2019) reports chemical products

694   (partially by extrapolating composition measurements of others sizes, especially at higher time resolutions

695   and lower concentrations), covers 76% (83%) and 11% (5%) of the AMP volume and number,

696   respectively.

697   To complete the illustration of the coverage of the previously discussed instruments, the vertical

698   profiles of observed volume fractions, in both the submicron range and the full AMP size range, are

699   summarized in Fig. 9 (and the statistics summarized in Table S2 in SI). For the submicron measurements,

700   AMS is highly comparable to the URG PM$_1$ standard cut cyclone, MOUDI 1 µm stage impactor, and

701   SAGA MC. More particle volume is observed by AMS as altitude increases, due to the relatively constant

702   AMS lens transmission (that always operates in the free molecular regime) and the smaller aerodynamic

703   cutoff sizes for the other three inlets (that operate at ambient P). For the AMP size range, similar

704   increasing fractions of V_{phys} as a function of altitude are observed in all the panels, except for PALMS-

705   AMP, due to the larger fraction of the aerosol population at smaller diameters aloft than at the surface

706   (Fig. 8) (Williamson et al. 2019). PALMS excels in the lower 2 km of the atmosphere where it

707   characterizes most of the volume, while the submicron instruments only capture ~40-50 %. This clearly

708   shows the heterogeneity and complementarity between PALMS-AMP and the other submicron bulk

709 measurements as a function of altitude. The differences between the 3 min characterization and the

710 PALMS-AMP products are greatly reduced by averaging to 60 min.

711   In summary, outside dust or biomass burning plumes, the particle volume sampled by AMS is

712 within $97 \pm 14\%$ compared to SAGA MC, for which the difference disappears for the higher altitude legs,

713 and $85 \pm 10\%$ of an airborne dry PM_1 measurement, a MOUDI impactor often used in aircraft. AMS and

714 PALMS particle compositional data overlap for a large part of the volume distribution in ATom, and they

715 complement each other at the ends of the distribution (the statistics of the overlap are listed in Table S2).

716 Last but not the least, SAGA filters characterize the particle bulk chemical components representative of

717 the combined size range from the NOAA particle spectrometers.

718 **4 Conclusion**

719   The large range of conditions sampled by the high-quality aerosol instrument payload onboard the

720 NASA DC-8 during the ATom missions provides unique opportunity to quantitatively investigate the

721 comparability of submicron volume (and hence mass quantification) derived from physical sizing vs. bulk

722 chemical instruments, as well as to evaluate whether currently reported AMS measurement uncertainties

723 are realistic. Characterizing the upper end of the AMS transmission curve during field deployments is

724 critical for meaningful intercomparisons. Calibrating the AMS transmission curve avoids improperly

725 attributing the differences in transmission to errors in *CE* or *RIE* if a discrepancy is found. In-field

726 calibration of AMS transmission is suggested since lens alignment or possible impacts during transport

727 have been observed to cause a change in transmission. AMS variability in transmission can be significant,

728 e.g., this study vs. Hu et al. (2017) and Liu et al. (2007), leading to differences of up to 25% in transmitted

729 concentrations for ATom conditions, which could be larger in the presence of a larger accumulation mode.

730 After applying the AMS transmission curve to the size spectrometer data, good agreement was found

731 between the physically and chemically derived volumes over three orders-of-magnitude (slope = 0.96 and

732 1.09, r^2 = 0.95 and 0.93, for ATom-1 and -2, respectively). Significant deviations would have been

733 observed if some literature transmission curves had been used. No evidence of biases in AMS detection

734 of remote aerosols was found. The combined stated uncertainties are consistent for the overall statistics

735 of the instrument comparison for the remote aerosols sampled during ATom.

736   The CU AMS inlet was equivalent to a $PM_{0.75}$ cyclone operating on ambient particles (i.e., not

737   dried prior to sampling) during ATom-1 to -3 and to a $PM_{0.95}$ cyclone during ATom-4. For an aerosol

738   density of 0.9 g cm^{-3}, such as pure hydrocarbon-like OA or cooking aerosol dominated by fatty acids, the

739   same AMS is equivalent to a $PM_{0.79}$ (ATom-1, -2, -3) and $PM_{1.0}$ (ATom-4) cyclone for dry particles.

740   Despite being equivalent to a $PM_{0.75}$ cyclone in ATom-1 and -2, $95 \pm 15\%$ of the theoretically calculated

741   URG PM_1 cyclone sampled mass/volume was detected by the AMS, as the effect of ambient pressure and

742   humidity on the URG cyclone transmission bridges the gap. Furthermore, the AMS quantified particle

743   mass and properties represent 68% (mean) of the integrated AMP volume and 41% of the integrated AMP

744   number from 2.7 nm to 4.8 µm geometric diameter (d_p) size range. PALMS-AMP at a 3-min time

745   resolution (or the PALMS-AMP products, which assumes a full coverage of >100 nm d_p AMP)

746   characterizes 54% (76%) of the integrated volume and 5% (11%) of the integrated number, while MOUDI

747   1 µm stage impactor would collect 78% of the volume and 89% of the number. SAGA filters collect

748   nearly all the aerosol, 96% of the volume and 98% of the number. The more pressure-dependent cutoff

749   size of MOUDI or similar inlet that operates at ambient P for airborne sampling may impact comparisons

750   with data from other instruments as a function of altitude. That effect could be compensated by lowering

751   the volumetric flow rate vs. altitude to keep the size cut (i.e., d_{50}) the same at the cost of a less sharp

752   transmission. The CU AMS inlet provides a more constant transmission vs. altitude. This work serves as

753   a case study of the importance of size ranges when intercomparing different instruments, and contributes

754   to document the performance of the ATom aerosol payload, confirms the realism of the stated

755   uncertainties, and serves as a framework for a subsequent intercomparison focusing on individual

756   chemical species.

757

Atmospheric
Measurement
Techniques
Discussions

Open Access

EGU

764 and Agnieszka Kupc for the use of the AMP data, Joshua Schwarz and Joseph Katich for use of the SP2

765 data, and Karl Froyd and Daniel Murphy for useful discussions about PALMS.

766

767 *Data availability.* The ATom data is published at https://doi.org/10.3334/ORNLDAAC/1581.

768 **References**

769 ACTRiS: ACTRiS Data Centre, [online] Available from:
770 https://www.actris.eu/DataServices/Data/DataCentre.aspx (Accessed 15 November 2019), 2019.

771 Aldhaif, A. M., Stahl, C., Braun, R. A., Moghaddam, M. A., Shingler, T., Crosbie, E., Sawamura, P.,
772 Dadashazar, H., Ziemba, L., Jimenez, J. L., Campuzano-Jost, P. and Sorooshian, A.: Characterization of
773 the Real Part of Dry Aerosol Refractive Index Over North America From the Surface to 12 km, J.
774 Geophys. Res. Atmos., 123(15), 8283–8300, 2018.

775 Alfarra, M. R., Coe, H., Allan, J. D., Bower, K. N., Boudries, H., Canagaratna, M. R., Jimenez, J. L.,
776 Jayne, J. T., Garforth, A. A., Li, S.-M. and Worsnop, D. R.: Characterization of urban and rural organic
777 particulate in the Lower Fraser Valley using two Aerodyne Aerosol Mass Spectrometers, Atmos.
778 Environ., 38(34), 5745–5758, 2004.

779 Bahreini, R., Dunlea, E. J., Matthew, B. M., Simons, C., Docherty, K. S., DeCarlo, P. F., Jimenez, J. L.,
780 Brock, C. A. and Middlebrook, A. M.: Design and Operation of a Pressure-Controlled Inlet for Airborne
781 Sampling with an Aerodynamic Aerosol Lens, Aerosol Sci. Technol., 42(6), 465–471, 2008.

782 Bahreini, R., Ervens, B., Middlebrook, A. M., Warneke, C., de Gouw, J. A., DeCarlo, P. F., Jimenez, J.
783 L., Brock, C. A., Neuman, J. A., Ryerson, T. B., Stark, H., Atlas, E., Brioude, J., Fried, A., Holloway, J.
784 S., Peischl, J., Richter, D., Walega, J., Weibring, P., Wollny, A. G. and Fehsenfeld, F. C.: Organic aerosol
785 formation in urban and industrial plumes near Houston and Dallas, Texas, J. Geophys. Res., 114, D00F16,
786 2009.

787 Barth, M. C., Cantrell, C. A., Brune, W. H., Rutledge, S. A., Crawford, J. H., Huntrieser, H., Carey, L.
788 D., MacGorman, D., Weisman, M., Pickering, K. E., Bruning, E., Anderson, B., Apel, E., Biggerstaff,
789 M., Campos, T., Campuzano-Jost, P., Cohen, R., Crounse, J., Day, D. A., Diskin, G., Flocke, F., Fried,
790 A., Garland, C., Heikes, B., Honomichl, S., Hornbrook, R., Huey, L. G., Jimenez, J. L., Lang, T.,
791 Lichtenstern, M., Mikoviny, T., Nault, B., O'Sullivan, D., Pan, L. L., Peischl, J., Pollack, I., Richter, D.,
792 Riemer, D., Ryerson, T., Schlager, H., St. Clair, J., Walega, J., Weibring, P., Weinheimer, A., Wennberg,
793 P., Wisthaler, A., Wooldridge, P. J. and Ziegler, C.: The Deep Convective Clouds and Chemistry (DC3)
794 Field Campaign, Bull. Am. Meteorol. Soc., 96(8), 1281–1309, 2015.

795 Brock, C. A., Cozic, J., Bahreini, R., Froyd, K. D., Middlebrook, A. M., McComiskey, A., Brioude, J.,
796 Cooper, O. R., Stohl, A., Aikin, K. C., Gouw, J. A. de, Fahey, D. W., Ferrare, R. A., Gao, R.-S., Gore,

Atmospheric
Measurement
Techniques
Discussions

Open Access
EGU

W., Holloway, J. S., Hübler, G., Jefferson, A., Lack, D. A., Lance, S., Moore, R. H., Murphy, D. M., Nenes, A., Novelli, P. C., Nowak, J. B., Ogren, J. A., Peischl, J., Pierce, R. B., Pilewskie, P., Quinn, P. K., Ryerson, T. B., Schmidt, K. S., Schwarz, J. P., Sodemann, H., Spackman, J. R., Stark, H., Thomson, D. S., Thornberry, T., Veres, P., Watts, L. A., Warneke, C. and Wollny, A. G.: Characteristics, sources, and transport of aerosols measured in spring 2008 during the Aerosol, Radiation, and Cloud Processes Affecting Arctic Climate (ARCPAC) Project, Atmos. Chem. Phys., 11(6), 2423–2453, 2011.

Brock, C. A., Williamson, C., Kupc, A., Froyd, K. D., Erdesz, F., Wagner, N., Richardson, M., Schwarz, J. P., Gao, R.-S., Katich, J. M., Campuzano-Jost, P., Nault, B. A., Schroder, J. C., Jimenez, J. L., Weinzierl, B., Dollner, M., Bui, T. and Murphy, D. M.: Aerosol size distributions during the Atmospheric Tomography Mission (ATom): methods, uncertainties, and data products, Atmos. Meas. Tech., 12(6), 3081–3099, 2019.

Campuzano-Jost, P.: Some useful customizations of the AMS: Developing an internal calibrant standard, integrating a cryopump to the ionization chamber, and a custom vent assembly, [online] Available from: http://cires1.colorado.edu/jimenez-group/UsrMtgs/UsersMtg13/2012_TechPres_PCJ.pdf, 2012.

Canagaratna, M. R., Jayne, J. T., Jimenez, J. L., Allan, J. D., Alfarra, M. R., Zhang, Q., Onasch, T. B., Drewnick, F., Coe, H., Middlebrook, A., Delia, A., Williams, L. R., Trimborn, A. M., Northway, M. J., DeCarlo, P. F., Kolb, C. E., Davidovits, P. and Worsnop, D. R.: Chemical and microphysical characterization of ambient aerosols with the aerodyne aerosol mass spectrometer, Mass Spectrom. Rev., 26(2), 185–222, 2007.

Canagaratna, M. R., Jimenez, J. L., Kroll, J. H., Chen, Q., Kessler, S. H., Massoli, P., Hildebrandt Ruiz, L., Fortner, E., Williams, L. R., Wilson, K. R., Surratt, J. D., Donahue, N. M., Jayne, J. T. and Worsnop, D. R.: Elemental ratio measurements of organic compounds using aerosol mass spectrometry: characterization, improved calibration, and implications, Atmos. Chem. Phys., 15(1), 253–272, 2015.

Crenn, V., Sciare, J., Croteau, P. L., Verlhac, S., Fröhlich, R., Belis, C. A., Aas, W., Äijälä, M., Alastuey, A., Artiñano, B., Baisnée, D., Bonnaire, N., Bressi, M., Canagaratna, M., Canonaco, F., Carbone, C., Cavalli, F., Coz, E., Cubison, M. J., Esser-Gietl, J. K., Green, D. C., Gros, V., Heikkinen, L., Herrmann, H., Lunder, C., Minguillón, M. C., Močnik, G., O'Dowd, C. D., Ovadnevaite, J., Petit, J.-E., Petralia, E., Poulain, L., Priestman, M., Riffault, V., Ripoll, A., Sarda-Estève, R., Slowik, J. G., Setyan, A., Wiedensohler, A., Baltensperger, U., Prévôt, A. S. H., Jayne, J. T. and Favez, O.: ACTRIS ACSM intercomparison – Part 1: Reproducibility of concentration and fragment results from 13 individual Quadrupole Aerosol Chemical Speciation Monitors (Q-ACSM) and consistency with co-located instruments, Atmos. Meas. Tech., 8(12), 5063–5087, 2015.

Cubison, M. J., Ortega, A. M., Hayes, P. L., Farmer, D. K., Day, D., Lechner, M. J., Brune, W. H., Apel, E., Diskin, G. S., Fisher, J. A., Fuelberg, H. E., Hecobian, A., Knapp, D. J., Mikoviny, T., Riemer, D., Sachse, G. W., Sessions, W., Weber, R. J., Weinheimer, A. J., Wisthaler, A. and Jimenez, J. L.: Effects of aging on organic aerosol from open biomass burning smoke in aircraft and laboratory studies, Atmos. Chem. Phys., 11(23), 12049–12064, 2011.

Atmospheric
Measurement
Techniques
Discussions
Open Access

EGU

834 DeCarlo, P. F., Slowik, J. G., Worsnop, D. R., Davidovits, P. and Jimenez, J. L.: Particle Morphology
835 and Density Characterization by Combined Mobility and Aerodynamic Diameter Measurements. Part 1:
836 Theory, Aerosol Sci. Technol., 38(12), 1185–1205, 2004.

837 DeCarlo, P. F., Kimmel, J. R., Trimborn, A., Northway, M. J., Jayne, J. T., Aiken, A. C., Gonin, M.,
838 Fuhrer, K., Horvath, T., Docherty, K. S., Worsnop, D. R. and Jimenez, J. L.: Field-deployable, high-
839 resolution, time-of-flight aerosol mass spectrometer, Anal. Chem., 78(24), 8281–8289, 2006.

840 DeCarlo, P. F., Dunlea, E. J., Kimmel, J. R., Aiken, A. C., Sueper, D., Crounse, J., Wennberg, P. O.,
841 Emmons, L., Shinozuka, Y., Clarke, A., Zhou, J., Tomlinson, J., Collins, D. R., Knapp, D., Weinheimer,
842 A. J., Montzka, D. D., Campos, T. and Jimenez, J. L.: Fast airborne aerosol size and chemistry
843 measurements above Mexico City and Central Mexico during the MILAGRO campaign, Atmos. Chem.
844 Phys., 8(14), 4027–4048, 2008.

845 DeCarlo, P. F., Ulbrich, I. M., Crounse, J., de Foy, B., Dunlea, E. J., Aiken, A. C., Knapp, D., Weinheimer,
846 A. J., Campos, T., Wennberg, P. O. and Jimenez, J. L.: Investigation of the sources and processing of
847 organic aerosol over the Central Mexican Plateau from aircraft measurements during MILAGRO, Atmos.
848 Chem. Phys., 10(12), 5257–5280, 2010.

849 Dibb, J. E.: ATom: Measurements of Soluble Acidic Gases and Aerosols (SAGA), ,
850 doi:10.3334/ORNLDAAC/1748, 2019.

851 Dibb, J. E., Talbot, R. W., Scheuer, E. M., Blake, D. R., Blake, N. J., Gregory, G. L., Sachse, G. W. and
852 Thornton, D. C.: Aerosol chemical composition and distribution during the Pacific Exploratory Mission
853 (PEM) Tropics, J. Geophys. Res. Atmos., 104(D5), 5785–5800, 1999.

854 Dibb, J. E., Talbot, R. W. and Scheuer, E. M.: Composition and distribution of aerosols over the North
855 Atlantic during the Subsonic Assessment Ozone and Nitrogen Oxide Experiment (SONEX), J. Geophys.
856 Res. Atmos., 105(D3), 3709–3717, 2000.

857 Docherty, K. S., Aiken, A. C., Huffman, J. A., Ulbrich, I. M., DeCarlo, P. F., Sueper, D., Worsnop, D.
858 R., Snyder, D. C., Peltier, R. E., Weber, R. J., Grover, B. D., Eatough, D. J., Williams, B. J., Goldstein,
859 A. H., Ziemann, P. J. and Jimenez, J. L.: The 2005 Study of Organic Aerosols at Riverside (SOAR-1):
860 instrumental intercomparisons and fine particle composition, Atmos. Chem. Phys., 11(23), 12387–12420,
861 2011.

862 van Donkelaar, A., Martin, R. V., Leaitch, W. R., Macdonald, A. M., Walker, T. W., Streets, D. G.,
863 Zhang, Q., Dunlea, E. J., Jimenez, J. L., Dibb, J. E., Huey, L. G., Weber, R. and Andreae, M. O.: Analysis
864 of aircraft and satellite measurements from the Intercontinental Chemical Transport Experiment (INTEX-
865 B) to quantify long-range transport of East Asian sulfur to Canada, Atmos. Chem. Phys., 8(11), 2999–
866 3014, 2008.

867 Drewnick, F., Hings, S. S., DeCarlo, P., Jayne, J. T., Gonin, M., Fuhrer, K., Weimer, S., Jimenez, J. L.,

Atmospheric
Measurement
Techniques
Discussions

868 Demerjian, K. L., Borrmann, S. and Worsnop, D. R.: A New Time-of-Flight Aerosol Mass Spectrometer
869 (TOF-AMS)—Instrument Description and First Field Deployment, Aerosol Sci. Technol., 39(7), 637–
870 658, 2005.

871 Drewnick, F., Hings, S. S., Alfarra, M. R., Prevot, A. S. H. and Borrmann, S.: Aerosol quantification with
872 the Aerodyne Aerosol Mass Spectrometer: detection limits and ionizer background effects, Atmos. Meas.
873 Tech., 2(1), 33–46, 2009.

874 Dunlea, E. J., DeCarlo, P. F., Aiken, A. C., Kimmel, J. R., Peltier, R. E., Weber, R. J., Tomlinson, J.,
875 Collins, D. R., Shinozuka, Y., McNaughton, C. S., Howell, S. G., Clarke, A. D., Emmons, L. K., Apel,
876 E. C., Pfister, G. G., van Donkelaar, A., Martin, R. V., Millet, D. B., Heald, C. L. and Jimenez, J. L.:
877 Evolution of Asian aerosols during transpacific transport in INTEX-B, Atmos. Chem. Phys., 9(19), 7257–
878 7287, 2009.

879 Dzepina, K., Arey, J., Marr, L. C., Worsnop, D. R., Salcedo, D., Zhang, Q., Onasch, T. B., Molina, L. T.,
880 Molina, M. J. and Jimenez, J. L.: Detection of particle-phase polycyclic aromatic hydrocarbons in Mexico
881 City using an aerosol mass spectrometer, Int. J. Mass Spectrom., 263(2), 152–170, 2007.

882 Farmer, D. K., Matsunaga, A., Docherty, K. S., Surratt, J. D., Seinfeld, J. H., Ziemann, P. J. and Jimenez,
883 J. L.: Response of an aerosol mass spectrometer to organonitrates and organosulfates and implications for
884 atmospheric chemistry, Proc. Natl. Acad. Sci. U.S.A., 107(15), 6670–6675, 2010.

885 Froyd, K. D., Murphy, D. M., Brock, C. A., Campuzano-Jost, P., Dibb, J. E., Jimenez, J. L., Kupc, A.,
886 Middlebrook, A. M., Schill, G. P., Thornhill, K. L., Williamson, C. J., Wilson, J. C. and Ziemba, L. D.:
887 A new method to quantify mineral dust and other aerosol species from aircraft platforms using single-
888 particle mass spectrometry, Atmos. Meas. Tech., 12(11), 6209–6239, 2019.

889 Garofalo, L. A., Pothier, M. A., Levin, E. J. T., Campos, T., Kreidenweis, S. M. and Farmer, D. K.:
890 Emission and Evolution of Submicron Organic Aerosol in Smoke from Wildfires in the Western United
891 States, ACS Earth Space Chem., 3(7), 1237–1247, 2019.

892 Guo, H., Sullivan, A. P., Campuzano-Jost, P., Schroder, J. C., Lopez-Hilfiker, F. D., Dibb, J. E., Jimenez,
893 J. L., Thornton, J. A., Brown, S. S., Nenes, A. and Weber, R. J.: Fine particle pH and the partitioning of
894 nitric acid during winter in the northeastern United States, J. Geophys. Res.: Atmos., 121(17), 10355–
895 10376, 2016.

896 Haywood, J. and Boucher, O.: Estimates of the direct and indirect radiative forcing due to tropospheric
897 aerosols: A review, Rev. Geophys., 38(4), 513–543, 2000.

898 Heim, E. W., Dibb, J., Scheuer, E., Campuzano Jost, P., Nault, B. A., Jimenez, J. L., Peterson, D., Knote,
899 C., Fenn, M., Hair, J., Beyersdorf, A. J., Corr, C. and Anderson, B. E.: Asian dust observed during
900 KORUS-AQ facilitates the uptake and incorporation of soluble pollutants during transport to South
901 Korea, Atmos. Environ., 224, 117305, 2020.

Atmospheric
Measurement
Techniques
Discussions

Open Access

EGU

Herring, C. L., Faiola, C. L., Massoli, P., Sueper, D., Erickson, M. H., McDonald, J. D., Simpson, C. D., Yost, M. G., Jobson, B. T. and VanReken, T. M.: New Methodology for Quantifying Polycyclic Aromatic Hydrocarbons (PAHs) Using High-Resolution Aerosol Mass Spectrometry, Aerosol Sci. Technol., 49(11), 1131–1148, 2015.

Hodzic, A., Campuzano-Jost, P., Bian, H., Chin, M., Colarco, P. R., Day, D. A., Froyd, K. D., Heinold, B., Jo, D. S., Katich, J. M., Kodros, J. K., Nault, B. A., Pierce, J. R., Ray, E., Schacht, J., Schill, G. P., Schroder, J. C., Schwarz, J. P., Sueper, D. T., Tegen, I., Tilmes, S., Tsigaridis, K., Yu, P. and Jimenez, J. L.: Characterization of organic aerosol across the global remote troposphere: a comparison of ATom measurements and global chemistry models, Atmos. Chem. Phys., 20(8), 4607–4635, 2020.

Huffman, J. A., Jayne, J. T., Drewnick, F., Aiken, A. C., Onasch, T., Worsnop, D. R. and Jimenez, J. L.: Design, Modeling, Optimization, and Experimental Tests of a Particle Beam Width Probe for the Aerodyne Aerosol Mass Spectrometer, Aerosol Sci. Technol., 39(12), 1143–1163, 2005.

Hu, W., Campuzano-Jost, P., Day, D. A., Croteau, P., Canagaratna, M. R., Jayne, J. T., Worsnop, D. R. and Jimenez, J. L.: Evaluation of the new capture vaporizer for aerosol mass spectrometers (AMS) through field studies of inorganic species, Aerosol Sci. Technol., 51(6), 735–754, 2017.

Hu, W., Day, D. A., Campuzano-Jost, P., Nault, B. A., Park, T., Lee, T., Croteau, P., Canagaratna, M. R., Jayne, J. T., Worsnop, D. R. and Jimenez, J. L.: Evaluation of the New Capture Vaporizer for Aerosol Mass Spectrometers (AMS): Elemental Composition and Source Apportionment of Organic Aerosols (OA), ACS Earth Space Chem., 2(4), 410–421, 2018.

Hu, W., Campuzano-Jost, P., Day, D. A., Nault, B. A., Park, T., Lee, T., Pajunoja, A., Virtanen, A., Croteau, P., Canagaratna, M. R., Jayne, J. T., Worsnop, D. R. and Jimenez, J. L.: Ambient Quantification and Size Distributions for Organic Aerosol in Aerosol Mass Spectrometers with the New Capture Vaporizer, ACS Earth Space Chem., 4(5), 676–689, 2020.

Hu, W. W., Campuzano-Jost, P., Palm, B. B., Day, D. A., Ortega, A. M., Hayes, P. L., Krechmer, J. E., Chen, Q., Kuwata, M., Liu, Y. J., Sá, S. S. de, McKinney, K., Martin, S. T., Hu, M., Budisulistiorini, S. H., Riva, M., Surratt, J. D., Clair, J. M. S., Isaacman-Van Wertz, G., Yee, L. D., Goldstein, A. H., Carbone, S., Brito, J., Artaxo, P., Gouw, J. A. de, Koss, A., Wisthaler, A., Mikoviny, T., Karl, T., Kaser, L., Jud, W., Hansel, A., Docherty, K. S., Alexander, M. L., Robinson, N. H., Coe, H., Allan, J. D., Canagaratna, M. R., Paulot, F. and Jimenez, J. L.: Characterization of a real-time tracer for isoprene epoxydiols-derived secondary organic aerosol (IEPOX-SOA) from aerosol mass spectrometer measurements, Atmos. Chem. Phys., 15(20), 11807–11833, 2015.

IPCC: Climate Change 2013: The Physical Science Basis. Contribution of Working Group I to the Fifth Assessment Report of the Intergovernmental Panel on Climate Change [Stocker, T.F., D. Qin, G.-K. Plattner, M. Tignor, S.K. Allen, J. Boschung, A. Nauels, Y. Xia, V. Bex and P.M. Midgley (eds.)], Cambridge University Press, Cambridge, United Kingdom and New York, NY, USA, 1535 pp., 2013.

Jayne, J.: Update on (AMS) Hardware since Last Year & Future Plans, [online] Available from: http://cires1.colorado.edu/jimenez-group/UsrMtgs/UsersMtg5/Presentations/JayneHardware.pdf, 2004.

Jayne, J. T., Leard, D. C., Zhang, X., Davidovits, P., Smith, K. A., Kolb, C. E. and Worsnop, D. R.: Development of an Aerosol Mass Spectrometer for Size and Composition Analysis of Submicron Particles, Aerosol Sci. Technol., 33(1-2), 49–70, 2000.

Jimenez, J. L., Jayne, J. T., Shi, Q., Kolb, C. E., Worsnop, D. R., Yourshaw, I., Seinfeld, J. H., Flagan, R. C., Zhang, X., Smith, K. A., Morris, J. W. and Davidovits, P.: Ambient aerosol sampling using the Aerodyne Aerosol Mass Spectrometer, J. Geophys. Res., 108(D7), 8425, 2003.

Jimenez, J. L., Canagaratna, M. R., Donahue, N. M., Prevot, A. S. H., Zhang, Q., Kroll, J. H., DeCarlo, P. F., Allan, J. D., Coe, H., Ng, N. L., Aiken, A. C., Docherty, K. S., Ulbrich, I. M., Grieshop, A. P., Robinson, A. L., Duplissy, J., Smith, J. D., Wilson, K. R., Lanz, V. A., Hueglin, C., Sun, Y. L., Tian, J., Laaksonen, A., Raatikainen, T., Rautiainen, J., Vaattovaara, P., Ehn, M., Kulmala, M., Tomlinson, J. M., Collins, D. R., Cubison, M. J., Dunlea, E. J., Huffman, J. A., Onasch, T. B., Alfarra, M. R., Williams, P. I., Bower, K., Kondo, Y., Schneider, J., Drewnick, F., Borrmann, S., Weimer, S., Demerjian, K., Salcedo, D., Cottrell, L., Griffin, R., Takami, A., Miyoshi, T., Hatakeyama, S., Shimono, A., Sun, J. Y., Zhang, Y. M., Dzepina, K., Kimmel, J. R., Sueper, D., Jayne, J. T., Herndon, S. C., Trimborn, A. M., Williams, L. R., Wood, E. C., Middlebrook, A. M., Kolb, C. E., Baltensperger, U. and Worsnop, D. R.: Evolution of organic aerosols in the atmosphere, Science, 326(5959), 1525–1529, 2009.

Jimenez, J. L., Canagaratna, M. R., Drewnick, F., Allan, J. D., Alfarra, M. R., Middlebrook, A. M., Slowik, J. G., Zhang, Q., Coe, H., Jayne, J. T. and Worsnop, D. R.: Comment on "The effects of molecular weight and thermal decomposition on the sensitivity of a thermal desorption aerosol mass spectrometer," Aerosol Sci. Technol., 50(9), i–xv, 2016.

Katich, J. M., Samset, B. H., Bui, T. P., Dollner, M., Froyd, K. D., Campuzano-Jost, P., Nault, B. A., Schroder, J. C., Weinzierl, B. and Schwarz, J. P.: Strong Contrast in Remote Black Carbon Aerosol Loadings Between the Atlantic and Pacific Basins, J. Geophys. Res.: Atmos., 123(23), 13386–13395, 2018.

Kiendler-Scharr, A., Mensah, A. A., Friese, E., Topping, D., Nemitz, E., Prevot, A. S. H., Äijälä, M., Allan, J., Canonaco, F., Canagaratna, M., Carbone, S., Crippa, M., Dall Osto, M., Day, D. A., De Carlo, P., Di Marco, C. F., Elbern, H., Eriksson, A., Freney, E., Hao, L., Herrmann, H., Hildebrandt, L., Hillamo, R., Jimenez, J. L., Laaksonen, A., McFiggans, G., Mohr, C., O'Dowd, C., Otjes, R., Ovadnevaite, J., Pandis, S. N., Poulain, L., Schlag, P., Sellegri, K., Swietlicki, E., Tiitta, P., Vermeulen, A., Wahner, A., Worsnop, D. and Wu, H.-C.: Ubiquity of organic nitrates from nighttime chemistry in the European submicron aerosol, Geophys. Res. Lett., 43(14), 7735–7744, 2016.

Kimmel, J. R., Farmer, D. K., Cubison, M. J., Sueper, D., Tanner, C., Nemitz, E., Worsnop, D. R., Gonin, M. and Jimenez, J. L.: Real-time aerosol mass spectrometry with millisecond resolution, Int. J. Mass Spectrom., 303(1), 15–26, 2011.

973   Knote, C., Brunner, D., Vogel, H., Allan, J., Asmi, A., Äijälä, M., Carbone, S., Gon, H. D. van der,
974   Jimenez, J. L., Kiendler-Scharr, A., Mohr, C., Poulain, L., Prévôt, A. S. H., Swietlicki, E. and Vogel, B.:
975   Towards an online-coupled chemistry-climate model: evaluation of trace gases and aerosols in COSMO-
976   ART, Geosci. Model Dev., 4(4), 1077–1102, 2011.

977   Koenig, T. K., Baidar, S., Campuzano-Jost, P., Cuevas, C. A., Dix, B., Fernandez, R. P., Guo, H., Hall,
978   S. R., Kinnison, D., Nault, B. A., Ullmann, K., Jimenez, J. L., Saiz-Lopez, A. and Volkamer, R.:
979   Quantitative detection of iodine in the stratosphere, Proc. Natl. Acad. Sci. U.S.A., 117(4), 1860–1866,
980   2020.

981   Kupc, A., Williamson, C., Wagner, N. L., Richardson, M. and Brock, C. A.: Modification, calibration,
982   and performance of the Ultra-High Sensitivity Aerosol Spectrometer for particle size distribution and
983   volatility measurements during the Atmospheric Tomography Mission (ATom) airborne campaign,
984   Atmos. Meas. Tech., 11(1), 369–383, 2018.

985   Kuwata, M., Zorn, S. R. and Martin, S. T.: Using elemental ratios to predict the density of organic material
986   composed of carbon, hydrogen, and oxygen, Environ. Sci. Technol., 46(2), 787–794, 2012.

987   Liu, P. S. K., Deng, R., Smith, K. A., Williams, L. R., Jayne, J. T., Canagaratna, M. R., Moore, K.,
988   Onasch, T. B., Worsnop, D. R. and Deshler, T.: Transmission Efficiency of an Aerodynamic Focusing
989   Lens System: Comparison of Model Calculations and Laboratory Measurements for the Aerodyne
990   Aerosol Mass Spectrometer, Aerosol Sci. Technol., 41(8), 721–733, 2007.

991   Lohmann, U. and Feichter, J.: Global indirect aerosol effects: a review, Atmos. Chem. Phys., 5(3), 715–
992   733, 2005.

993   Marple, V., Olson, B., Romay, F., Hudak, G., Geerts, S. M. and Lundgren, D.: Second Generation Micro-
994   Orifice Uniform Deposit Impactor, 120 MOUDI-II: Design, Evaluation, and Application to Long-Term
995   Ambient Sampling, Aerosol Sci. Technol., 48(4), 427–433, 2014.

996   Marple, V. A., Rubow, K. L. and Behm, S. M.: A Microorifice Uniform Deposit Impactor (MOUDI):
997   Description, Calibration, and Use, Aerosol Sci. Technol., 14(4), 434–446, 1991.

998   Matthew, B. M., Middlebrook, A. M. and Onasch, T. B.: Collection Efficiencies in an Aerodyne Aerosol
999   Mass Spectrometer as a Function of Particle Phase for Laboratory Generated Aerosols, Aerosol Sci.
1000 Technol., 42(11), 884–898, 2008.

1001 McNaughton, C. S., Clarke, A. D., Howell, S. G., Pinkerton, M., Anderson, B., Thornhill, L., Hudgins,
1002 C., Winstead, E., Dibb, J. E., Scheuer, E. and Maring, H.: Results from the DC-8 Inlet Characterization
1003 Experiment (DICE): Airborne Versus Surface Sampling of Mineral Dust and Sea Salt Aerosols, Aerosol
1004 Sci. Technol., 41(2), 136–159, 2007.

1005 Mei, F., Hayes, P. L., Ortega, A., Taylor, J. W., Allan, J. D., Gilman, J., Kuster, W., de Gouw, J., Jimenez,

Atmospheric
Measurement
Techniques
Discussions

Open Access

EGU

J. L. and Wang, J.: Droplet activation properties of organic aerosols observed at an urban site during CalNex-LA, J. Geophys. Res.: Atmos., 118(7), 2903–2917, 2013.

Mei, F., Wang, J., Comstock, J. M., Weigel, R., Krämer, M., Mahnke, C., Shilling, J. E., Schneider, J., Schulz, C., Long, C. N., Wendisch, M., Machado, L. A. T., Schmid, B., Krisna, T., Pekour, M., Hubbe, J., Giez, A., Weinzierl, B., Zoeger, M., Pöhlker, M. L., Schlager, H., Cecchini, M. A., Andreae, M. O., Martin, S. T., de Sá, S. S., Fan, J., Tomlinson, J., Springston, S., Pöschl, U., Artaxo, P., Pöhlker, C., Klimach, T., Minikin, A., Afchine, A. and Borrmann, S.: Comparison of aircraft measurements during GoAmazon2014/5 and ACRIDICON-CHUVA, Atmos. Meas. Tech., 13(2), 661–684, 2020.

Middlebrook, A. M., Bahreini, R., Jimenez, J. L. and Canagaratna, M. R.: Evaluation of Composition-Dependent Collection Efficiencies for the Aerodyne Aerosol Mass Spectrometer using Field Data, Aerosol Sci. Technol., 46(3), 258–271, 2012.

Morgan, W. T., Allan, J. D., Bauguitte, S., Darbyshire, E., Flynn, M. J., Lee, J., Liu, D., Johnson, B., Haywood, J., Longo, K. M., Artaxo, P. E. and Coe, H.: Transformation and ageing of biomass burning carbonaceous aerosol over tropical South America from aircraft in situ measurements during SAMBBA, Atmos. Chem. Phys., 20, 5309–5326, 2020.

Murphy, D. M.: Reply to "Comment on the effects of molecular weight and thermal decomposition on the sensitivity of a thermal desorption aerosol mass spectrometer" by Jimenez et al, Aerosol Sci. Technol., 50(12), 1277–1283, 2016a.

Murphy, D. M.: The effects of molecular weight and thermal decomposition on the sensitivity of a thermal desorption aerosol mass spectrometer, Aerosol Sci. Technol., 50(2), 118–125, 2016b.

Murphy, D. M., Cziczo, D. J., Froyd, K. D., Hudson, P. K., Matthew, B. M., Middlebrook, A. M., Peltier, R. E., Sullivan, A., Thomson, D. S. and Weber, R. J.: Single-particle mass spectrometry of tropospheric aerosol particles, J. Geophys. Res., 111, D23S32, 2006.

Nault, B. A., Campuzano-Jost, P., Day, D. A., Schroder, J. C., Anderson, B., Beyersdorf, A. J., Blake, D. R., Brune, W. H., Choi, Y., Corr, C. A., Gouw, J. A. de, Dibb, J., DiGangi, J. P., Diskin, G. S., Fried, A., Huey, L. G., Kim, M. J., Knote, C. J., Lamb, K. D., Lee, T., Park, T., Pusede, S. E., Scheuer, E., Thornhill, K. L., Woo, J.-H. and Jimenez, J. L.: Secondary organic aerosol production from local emissions dominates the organic aerosol budget over Seoul, South Korea, during KORUS-AQ, Atmos. Chem. Phys., 18(24), 17769–17800, 2018.

Ng, N. L., Herndon, S. C., Trimborn, A., Canagaratna, M. R., Croteau, P. L., Onasch, T. B., Sueper, D., Worsnop, D. R., Zhang, Q., Sun, Y. L. and Jayne, J. T.: An Aerosol Chemical Speciation Monitor (ACSM) for Routine Monitoring of the Composition and Mass Concentrations of Ambient Aerosol, Aerosol Sci. Technol., 45(7), 780–794, 2011.

NOAA, NASA, U. S. Air Force: U. S. Standard Atmosphere 1976, U. S. Government Printing Office,

1040   Washington, DC., 1976.

1041   Ovadnevaite, J., Ceburnis, D., Canagaratna, M., Berresheim, H., Bialek, J., Martucci, G., Worsnop, D. R.
1042   and O'Dowd, C.: On the effect of wind speed on submicron sea salt mass concentrations and source
1043   fluxes, J. Geophys. Res.: Atmos, 117, D16201, 2012.

1044   Pajunoja, A., Hu, W., Leong, Y. J., Taylor, N. F., Miettinen, P., Palm, B. B., Mikkonen, S., Collins, D.
1045   R., Jimenez, J. L. and Virtanen, A.: Phase state of ambient aerosol linked with water uptake and chemical
1046   aging in the southeastern US, Atmos. Chem. Phys., 16(17), 11163–11176, 2016.

1047   Park, K., Kittelson, D. B., Zachariah, M. R. and McMurry, P. H.: Measurement of Inherent Material
1048   Density of Nanoparticle Agglomerates, J. Nanopart. Res., 6, 267–272, 2004.

1049   Peltier, R. E., Hecobian, A. H., Weber, R. J., Stohl, A., E. L. Atlas, Riemer, D. D., Blake, D. R., Apel, E.,
1050   Campos, T. and Karl, T.: Investigating the sources and atmospheric processing of fine particles from Asia
1051   and the Northwestern United States measured during INTEX B, Atmos. Chem. Phys., 8(6), 1835–1853,
1052   2008.

1053   Peters, T. M., Gussman, R. A., Kenny, L. C. and Vanderpool, R. W.: Evaluation of PM$_{2.5}$ Size Selectors
1054   Used in Speciation Samplers, Aerosol Sci. Technol., 34(5), 422–429, 2001.

1055   Petters, M. D., Prenni, A. J., Kreidenweis, S. M., DeMott, P. J., Matsunaga, A., Lim, Y. B. and Ziemann,
1056   P. J.: Chemical aging and the hydrophobic-to-hydrophilic conversion of carbonaceous aerosol, Geophys.
1057   Res. Lett., 33, L24806, 2006.

1058   Petzold, A., Ogren, J. A., Fiebig, M., Laj, P., Li, S.-M., Baltensperger, U., Holzer-Popp, T., Kinne, S.,
1059   Pappalardo, G., Sugimoto, N., Wehrli, C., Wiedensohler, A. and Zhang, X.-Y.: Recommendations for
1060   reporting "black carbon" measurements, Atmos. Chem. Phys., 13(16), 8365–8379, 2013.

1061   Pilinis, C., Pandis, S. N. and Seinfeld, J. H.: Sensitivity of direct climate forcing by atmospheric aerosols
1062   to aerosol size and composition, J. Geophys. Res., 100(D9), 18739–18754, 1995.

1063   Reyes-Villegas, E., Bannan, T., Le Breton, M., Mehra, A., Priestley, M., Percival, C., Coe, H. and Allan,
1064   J. D.: Online Chemical Characterization of Food-Cooking Organic Aerosols: Implications for Source
1065   Apportionment, Environ. Sci. Technol., 52(9), 5308–5318, 2018.

1066   Robinson, E. S., Onasch, T. B., Worsnop, D. and Donahue, N. M.: Collection efficiency of α-pinene
1067   secondary organic aerosol particles explored via light-scattering single-particle aerosol mass
1068   spectrometry, Atmos. Meas. Tech., 10(3), 1139–1154, 2017.

1069   Salcedo, D., Onasch, T. B., Dzepina, K., Canagaratna, M. R., Zhang, Q., Huffman, J. A., DeCarlo, P. F.,
1070   Jayne, J. T., Mortimer, P., Worsnop, D. R., Kolb, C. E., Johnson, K. S., Zuberi, B., Marr, L. C., Volkamer,
1071   R., Molina, L. T., Molina, M. J., Cardenas, B., Bernabé, R. M., Márquez, C., Gaffney, J. S., Marley, N.

Atmospheric
Measurement
Techniques
Discussions

A., Laskin, A., Shutthanandan, V., Xie, Y., Brune, W., Lesher, R., Shirley, T. and Jimenez, J. L.: Characterization of ambient aerosols in Mexico City during the MCMA-2003 campaign with Aerosol Mass Spectrometry: results from the CENICA Supersite, Atmos. Chem. Phys., 6(4), 925–946, 2006.

Salcedo, D., Onasch, T. B., Canagaratna, M. R., Dzepina, K., Huffman, J. A., Jayne, J. T., Worsnop, D. R., Kolb, C. E., Weimer, S., Drewnick, F., Allan, J. D., Delia, A. E. and Jimenez, J. L.: Technical Note: Use of a beam width probe in an Aerosol Mass Spectrometer to monitor particle collection efficiency in the field, Atmos. Chem. Phys., 7(2), 549–556, 2007.

Schroder, J. C., Campuzano-Jost, P., Day, D. A., Shah, V., Larson, K., Sommers, J. M., Sullivan, A. P., Campos, T., Reeves, J. M., Hills, A., Hornbrook, R. S., Blake, N. J., Scheuer, E., Guo, H., Fibiger, D. L., McDuffie, E. E., Hayes, P. L., Weber, R. J., Dibb, J. E., Apel, E. C., Jaeglé, L., Brown, S. S., Thornton, J. A. and Jimenez, J. L.: Sources and Secondary Production of Organic Aerosols in the Northeastern United States during WINTER, J. Geophys. Res. Atmos., 123, 7771–7796, 2018.

Schwarz, J. P., Spackman, J. R., Fahey, D. W., Gao, R. S., Lohmann, U., Stier, P., Watts, L. A., Thomson, D. S., Lack, D. A., Pfister, L., Mahoney, M. J., Baumgardner, D., Wilson, J. C. and Reeves, J. M.: Coatings and their enhancement of black carbon light absorption in the tropical atmosphere, J. Geophys. Res., 113(D3), 251, 2008.

Schwarz, J. P., Spackman, J. R., Gao, R. S., Watts, L. A., Stier, P., Schulz, M., Davis, S. M., Wofsy, S. C. and Fahey, D. W.: Global-scale black carbon profiles observed in the remote atmosphere and compared to models, Geophys. Res. Lett., 37, L18812, 2010a.

Schwarz, J. P., Spackman, J. R., Gao, R. S., Perring, A. E., Cross, E., Onasch, T. B., Ahern, A., Wrobel, W., Davidovits, P., Olfert, J., Dubey, M. K., Mazzoleni, C. and Fahey, D. W.: The Detection Efficiency of the Single Particle Soot Photometer, Aerosol Sci. Technol., 44(8), 612–628, 2010b.

Seinfeld, J. H. and Pandis, S. N.: Atmospheric Chemistry and Physics: From Air Pollution to Climate Change Third Edition, John Wiley & Sons., 2016.

Shilling, J. E., Chen, Q., King, S. M., Rosenoern, T., Kroll, J. H., Worsnop, D. R., DeCarlo, P. F., Aiken, A. C., Sueper, D., Jimenez, J. L. and Martin, S. T.: Loading-dependent elemental composition of α-pinene SOA particles, Atmos. Chem. Phys., 9(3), 771–782, 2009.

Shiraiwa, M., Kondo, Y., Moteki, N., Takegawa, N., Sahu, L. K., Takami, A., Hatakeyama, S., Yonemura, S. and Blake, D. R.: Radiative impact of mixing state of black carbon aerosol in Asian outflow, J. Geophys. Res., 113(D24), 1042, 2008.

Sloane, C. S., Watson, J., Chow, J., Pritchett, L. and Willard Richards, L.: Size-segregated fine particle measurements by chemical species and their impact on visibility impairment in Denver, Atmos. Environ. A-Gen., 25(5-6), 1013–1024, 1991.

Slowik, J. G., Stainken, K., Davidovits, P., Williams, L. R., Jayne, J. T., Kolb, C. E., Worsnop, D. R., Rudich, Y., DeCarlo, P. F. and Jimenez, J. L.: Particle Morphology and Density Characterization by Combined Mobility and Aerodynamic Diameter Measurements. Part 2: Application to Combustion-Generated Soot Aerosols as a Function of Fuel Equivalence Ratio, Aerosol Sci. Technol., 38(12), 1206–1222, 2004.

Stein, S. W., Turpin, B. J., Cai, X., Huang, P.-F. and Mcmurry, P. H.: Measurements of relative humidity-dependent bounce and density for atmospheric particles using the DMA-impactor technique, Atmos. Environ., 28(10), 1739–1746, 1994.

Stith, J. L., Ramanathan, V., Cooper, W. A., Roberts, G. C., DeMott, P. J., Carmichael, G., Hatch, C. D., Adhikary, B., Twohy, C. H., Rogers, D. C., Baumgardner, D., Prenni, A. J., Campos, T., Gao, R., Anderson, J. and Feng, Y.: An overview of aircraft observations from the Pacific Dust Experiment campaign, J. Geophys. Res., 114, D05207, 2009.

Takegawa, N., Miyazaki, Y., Kondo, Y., Komazaki, Y., Miyakawa, T., Jimenez, J. L., Jayne, J. T., Worsnop, D. R., Allan, J. D. and Weber, R. J.: Characterization of an Aerodyne Aerosol Mass Spectrometer (AMS): Intercomparison with Other Aerosol Instruments, Aerosol Sci. Technol., 39(8), 760–770, 2005.

Talbot, R., Dibb, J., Scheuer, E., Seid, G., Russo, R., Sandholm, S., Tan, D., Singh, H., Blake, D., Blake, N., Atlas, E., Sachse, G., Jordan, C. and Avery, M.: Reactive nitrogen in Asian continental outflow over the western Pacific: Results from the NASA Transport and Chemical Evolution over the Pacific (TRACE-P) airborne mission, J. Geophys. Res., 108(D20), 2171, 2003.

Thomson, D. S., Schein, M. E. and Murphy, D. M.: Particle Analysis by Laser Mass Spectrometry WB-57F Instrument Overview, Aerosol Sci. Technol., 33(1-2), 153–169, 2000.

Timonen, H., Aurela, M., Carbone, S., Saarnio, K., Saarikoski, S., Mäkelä, T., Kulmala, M., Kerminen, V.-M., Worsnop, D. R. and Hillamo, R.: High time-resolution chemical characterization of the water-soluble fraction of ambient aerosols with PILS-TOC-IC and AMS, Atmos. Meas. Tech., 3(4), 1063–1074, 2010.

Tsigaridis, K., Daskalakis, N., Kanakidou, M., Adams, P. J., Artaxo, P., Bahadur, R., Balkanski, Y., Bauer, S. E., Bellouin, N., Benedetti, A., Bergman, T., Berntsen, T. K., Beukes, J. P., Bian, H., Carslaw, K. S., Chin, M., Curci, G., Diehl, T., Easter, R. C., Ghan, S. J., Gong, S. L., Hodzic, A., Hoyle, C. R., Iversen, T., Jathar, S., Jimenez, J. L., Kaiser, J. W., Kirkevåg, A., Koch, D., Kokkola, H., H Lee, Y., Lin, G., Liu, X., Luo, G., Ma, X., Mann, G. W., Mihalopoulos, N., Morcrette, J.-J., Müller, J.-F., Myhre, G., Myriokefalitakis, S., Ng, N. L., O'donnell, D., Penner, J. E., Pozzoli, L., Pringle, K. J., Russell, L. M., Schulz, M., Sciare, J., Seland, Ø., Shindell, D. T., Sillman, S., Skeie, R. B., Spracklen, D., Stavrakou, T., Steenrod, S. D., Takemura, T., Tiitta, P., Tilmes, S., Tost, H., Van Noije, T., Van Zyl, P. G., Von Salzen, K., Yu, F., Wang, Z., Zaveri, R. A., Zhang, H., Zhang, K., Zhang, Q. and Zhang, X.: The AeroCom evaluation and intercomparison of organic aerosol in global models, Atmos. Chem. Phys., 14(19), 10845–

Atmospheric
Measurement
Techniques
Discussions

1141   10895, 2014.

1142   Vay, S. A., Anderson, B. E., Thornhill, K. L. and Hudgins, C. H.: An assessment of aircraft-generated
1143   contamination on in situ trace gas measurements: determinations from empirical data acquired aloft, J.
1144   Atmos. Ocean. Technol., 20(11), 1478–1487, 2003.

1145   Wang, J., Cubison, M. J., Aiken, A. C., Jimenez, J. L. and Collins, D. R.: The importance of aerosol
1146   mixing state and size-resolved composition on CCN concentration and the variation of the importance
1147   with atmospheric aging of aerosols, Atmos. Chem. Phys., 10(15), 7267–7283, 2010.

1148   Williamson, C., Kupc, A., Wilson, J., Gesler, D. W., Reeves, J. M., Erdesz, F., McLaughlin, R. and Brock,
1149   C. A.: Fast time response measurements of particle size distributions in the 3–60 nm size range with the
1150   nucleation mode aerosol size spectrometer, Atmos. Meas. Tech., 11(6), 3491–3509, 2018.

1151   Williamson, C. J., Kupc, A., Axisa, D., Bilsback, K. R., Bui, T., Campuzano-Jost, P., Dollner, M., Froyd,
1152   K. D., Hodshire, A. L., Jimenez, J. L., Kodros, J. K., Luo, G., Murphy, D. M., Nault, B. A., Ray, E. A.,
1153   Weinzierl, B., Wilson, J. C., Yu, F., Yu, P., Pierce, J. R. and Brock, C. A.: A large source of cloud
1154   condensation nuclei from new particle formation in the tropics, Nature, 574(7778), 399–403, 2019.

1155   Wofsy, S. C., Afshar, S., Allen, H. M., Apel, E., Asher, E. C., Barletta, B., Bent, J., Bian, H., Biggs, B.
1156   C., Blake, D. R., Blake, N., Bourgeois, I., Brock, C. A., Brune, W. H., Budney, J. W., Bui, T. P., Butler,
1157   A., Campuzano-Jost, P., Chang, C. S., Chin, M., Commane, R., Correa, G., Crounse, J. D., Cullis, P. D.,
1158   Daube, B. C., Day, D. A., Dean-Day, J. M., Dibb, J. E., Digangi, J. P., Diskin, G. S., Dollner, M., Elkins,
1159   J. W., Erdesz, F., Fiore, A. M., Flynn, C. M., Froyd, K., Gesler, D. W., Hall, S. R., Hanisco, T. F., Hannun,
1160   R. A., Hills, A. J., Hintsa, E. J., Hoffman, A., Hornbrook, R. S., Huey, L. G., Hughes, S., Jimenez, J. L.,
1161   Johnson, B. J., Katich, J. M., Keeling, R., Kim, M. J., Kupc, A., Lait, L. R., Lamarque, J.-F., Liu, J.,
1162   Mckain, K., Mclaughlin, R. J., Meinardi, S., Miller, D. O., Montzka, S. A., Moore, F. L., Morgan, E. J.,
1163   Murphy, D. M., Murray, L. T., Nault, B. A., Neuman, J. A., Newman, P. A., Nicely, J. M., Pan, X.,
1164   Paplawsky, W., Peischl, J., Prather, M. J., Price, D. J., Ray, E., Reeves, J. M., Richardson, M., Rollins,
1165   A. W., Rosenlof, K. H., Ryerson, T. B., Scheuer, E., Schill, G. P., Schroder, J. C., Schwarz, J. P., St. Clair,
1166   J. M., Steenrod, S. D., Stephens, B. B., Strode, S. A., Sweeney, C., Tanner, D., Teng, A. P., Thames, A.
1167   B., Thompson, C. R., Ullmann, K., Veres, P. R., Vizenor, N., Wagner, N. L., Watt, A., Weber, R.,
1168   Weinzierl, B., et al.: ATom: Merged Atmospheric Chemistry, Trace Gases, and Aerosols, ,
1169   doi:10.3334/ORNLDAAC/1581, 2018.

1170   Xu, W., Lambe, A., Silva, P., Hu, W., Onasch, T., Williams, L., Croteau, P., Zhang, X., Renbaum-Wolff,
1171   L., Fortner, E., Jimenez, J. L., Jayne, J., Worsnop, D. and Canagaratna, M.: Laboratory evaluation of
1172   species-dependent relative ionization efficiencies in the Aerodyne Aerosol Mass Spectrometer, Aerosol
1173   Sci. Technol., 52(6), 626–641, 2018.

1174   Zhang, Q., Stanier, C. O., Canagaratna, M. R., Jayne, J. T., Worsnop, D. R., Pandis, S. N. and Jimenez,
1175   J. L.: Insights into the chemistry of new particle formation and growth events in Pittsburgh based on
1176   aerosol mass spectrometry, Environ. Sci. Technol., 38(18), 4797–4809, 2004.

Atmospheric
Measurement
Techniques
Discussions

Open Access

Zhang, Q., Parworth, C., Lechner, M. and Jimenez, J. L.: Aerosol Mass Spectrometer (AMS) Global Database, [online] Available from: https://sites.google.com/site/amsglobaldatabase/ (Accessed 15 November 2019), 2018.
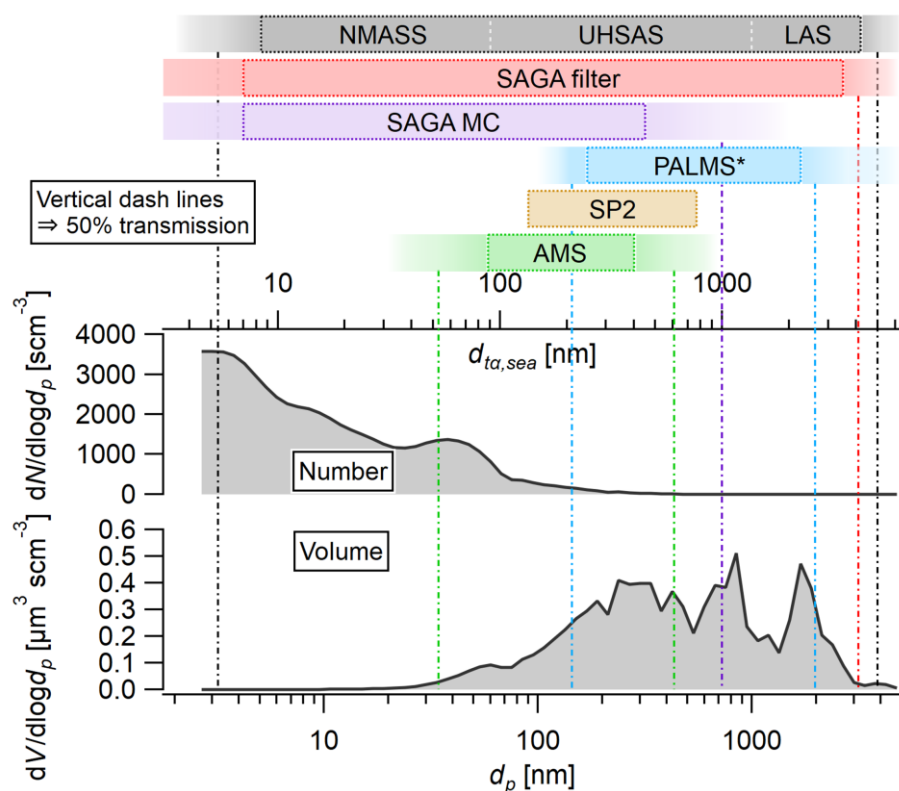
Figure 1: Approximate particle size ranges quantified by AMS, SP2, PALMS, SAGA MC, SAGA filters, and AMP (NMASS, UHSAS, and LAS), plotted with the campaign averaged AMP number and volume size distributions during ATom-2. For each instrument (except PALMS), the box indicates 100% inlet transmission and the transition shade on both sides indicates a decrease from 100% to 0%, with 50% denoted by the vertical dashed line. The PALMS bar represents the approximate size range contributing chemical information at a 60 min averaging time scale (at AMP size resolution) for composition data only (see Sect. 2.5). The top horizontal axis shows aerodynamic diameter ($d_{ta,sea}$) and the bottom geometric diameter (d_p); the conversion between the two diameters is based on ATom-2 campaign average aerosol density of 1.70 g cm^{-3} and sea level P of 1013 mbar using Eq. 2.
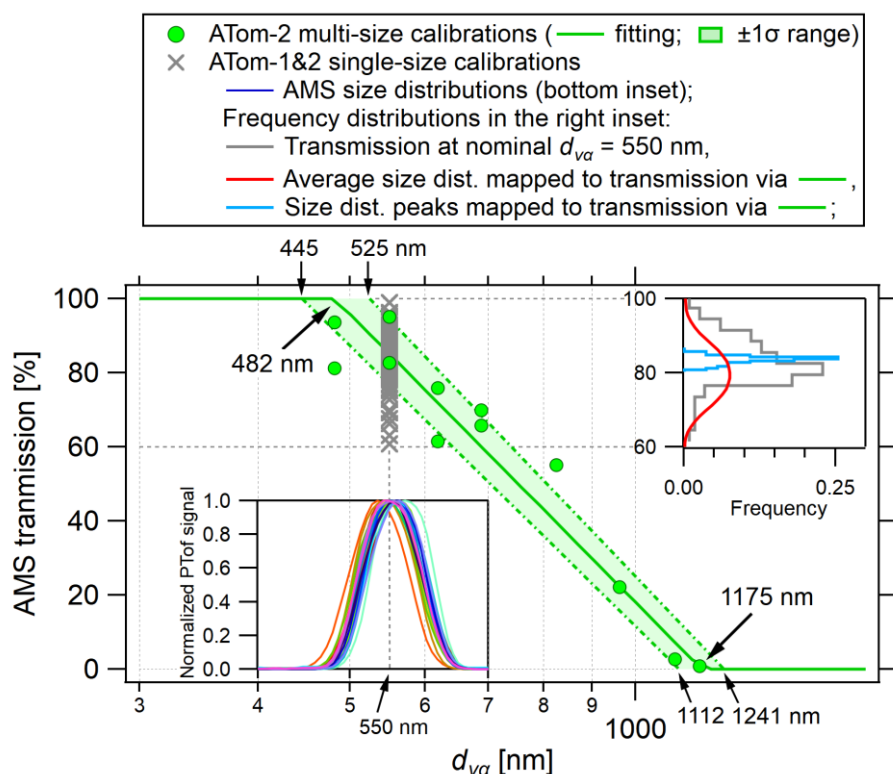
Figure 2: Results of in-field AMS large particle transmission calibrations vs. vacuum aerodynamic diameter (d_{va}) with NH_4NO_3 particles for ATom-1 and -2. The green markers are multi-size field calibrations, and the grey cross markers are single-size (at $d_m = 400$ nm, equivalent to 550 nm d_{va}) field calibrations after every research flight. The insets show the frequency distributions of measured transmissions (right, top) and observed, normalized size distributions (left, bottom) of these single-size calibrations. A fit shows 100% transmission at 483 nm (1σ uncertainty of the fit: 445-525 nm) and 0% transmission at 1175 nm (1σ: 1112-1241 nm). When forcing 0% transmission at 1175 nm (confirmed by $(NH_4)_2SO_4$ calibrations), the fit to all data gives 100% transmission at 482 nm (1σ: 479-485 nm, not shown), consistent with the 483 nm inferred based only on the ATom-2 multi-size field calibrations.
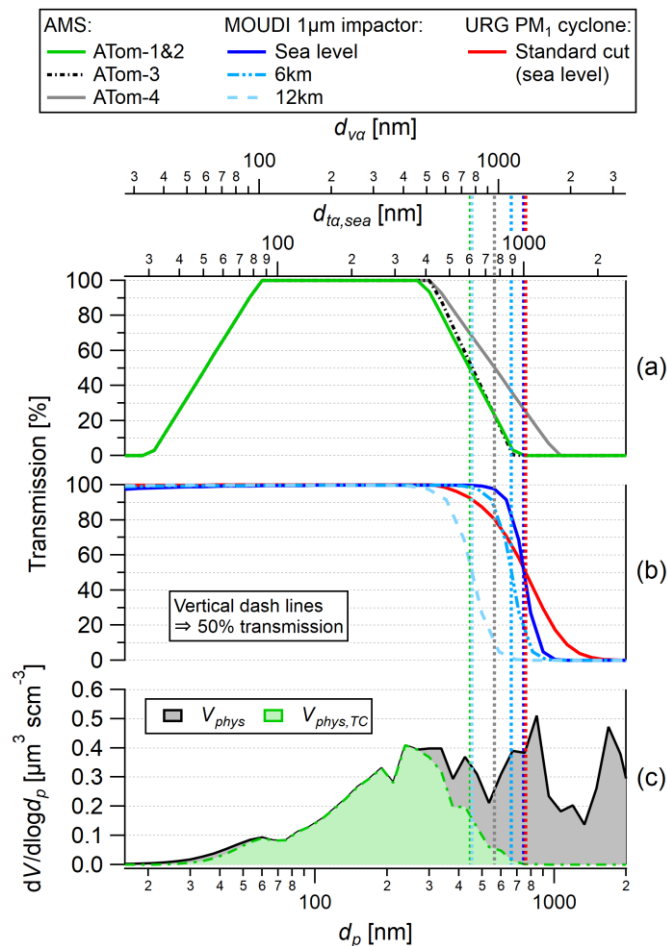
Figure 3: Transmission curves (a) for AMS during ATom-1 (same for ATom-2), -3 and -4 deployments, and (b) for MOUDI 1 μm stage impactor operated at sea level, 6 km, and 12 km (at $T = 293$ K as typical cabin temperature and P based on the U.S. standard atmosphere) (NOAA, NASA, U. S. Air Force, 1976), and for URG PM_1 cyclone (sea level). (c) Average NOAA volume distribution (V_{phys}) and the fraction observed by AMS ($V_{phys,TC}$) for ATom-2. Particle size in geometric diameter (d_p; reported by NOAA), vacuum aerodynamic diameter (d_{va}; AMS), and aerodynamic diameter (d_{ta}; for the MOUDI impactor and URG cyclone; note that the MOUDI transmissions at 6 and 12 km are accurate on the d_p and d_{va} axes, but slightly off on the sea level d_{ta} axis due to the change in slip correction) are shown as the three horizontal axes, all for dry particles. The 50% large particle cutoff sizes for AMS, MOUDI, and URG are listed in Table S1 based on d_{ta}, d_{va}, and d_p. Because URG cyclone is normally used to size-select ambient particles for ground studies, the equivalent dry cut would be smaller than 1 μm, approximately 0.8 μm based on the aerosols sampled in this study (Sect. 3.5).
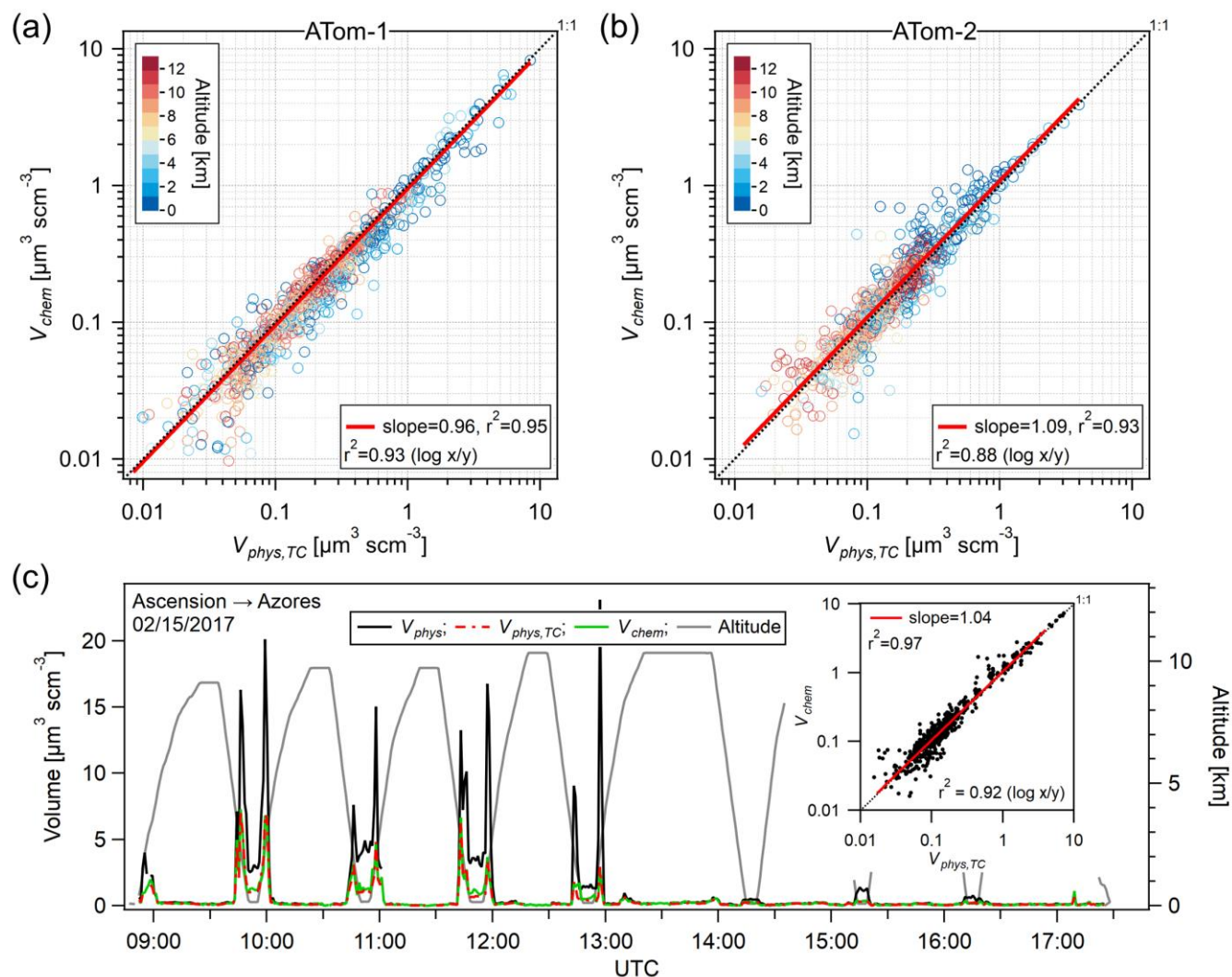
Figure 4: Comparison between V_{chem} and $V_{phys,TC}$ for (a) ATom-1 and (b) ATom-2, data points colored by altitude, and averaged to 5 min resolution. (c) A time series of the above two volumes as well as V_{phys} for a research flight in ATom-2, with an inset showing the scatter plot only for this flight (at 1 min time scale, as well as for the time series). Note that V_{chem} includes the AMS quantified sea salt. Two correlations coefficients (r^2) are listed: one at linear scale (commonly used) and the other at logarithmic scale, which emphasizes the scatter at low concentrations.

Atmospheric
Measurement
Techniques
Open Access
EGU
Discussions
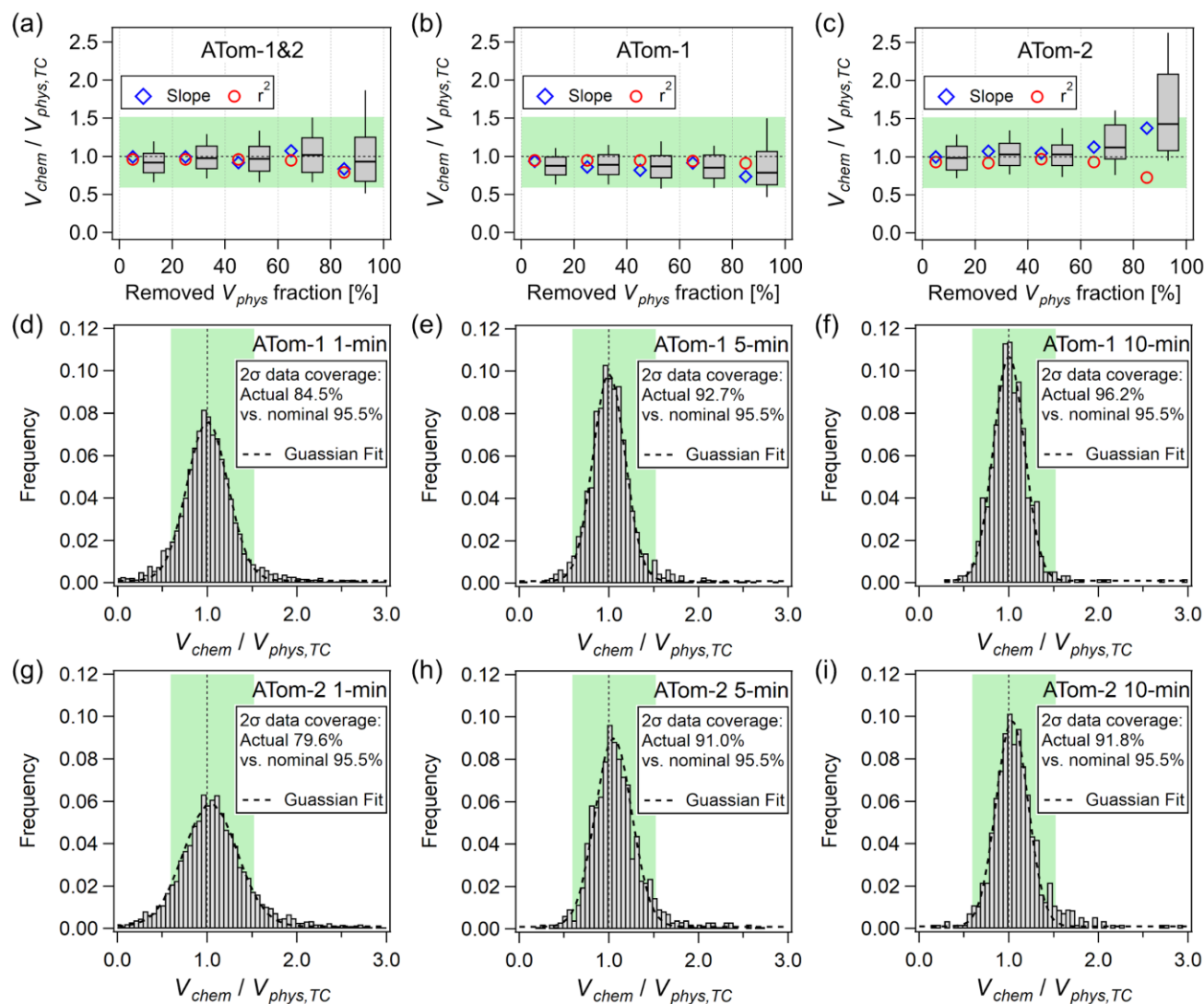
Figure 5: Box plots of $V_{chem}/V_{phys,TC}$, and the linear regression fitting slopes and correlations of the two volumes for (a) the combined ATom-1 and -2 data sets, (b) ATom-1, (c) ATom-2, binned by removed V_{phys} fraction when applying AMS transmission (at 20% interval). 10th, 25th, 50th, 75th, and 90th percentiles are plotted with the box and whiskers. The binned scatter plots can be found in SI as Fig. S20. (d-i) are the normalized frequency distributions of the volume ratio for ATom-1 and -2, respectively, at three averaging time scales: (left) 1 min, (middle) 5 min, and (right) 10 min. The green-tinted backgrounds indicate the combined 2σ accuracy from AMS (38%; 2σ) (Bahreini et al., 2009) and UHSAS (+12.4/-27.5%; treated as 1.5σ in this study) (Kupc et al., 2018).

Atmospheric
Measurement
Techniques
Open Access
Discussions
EGU
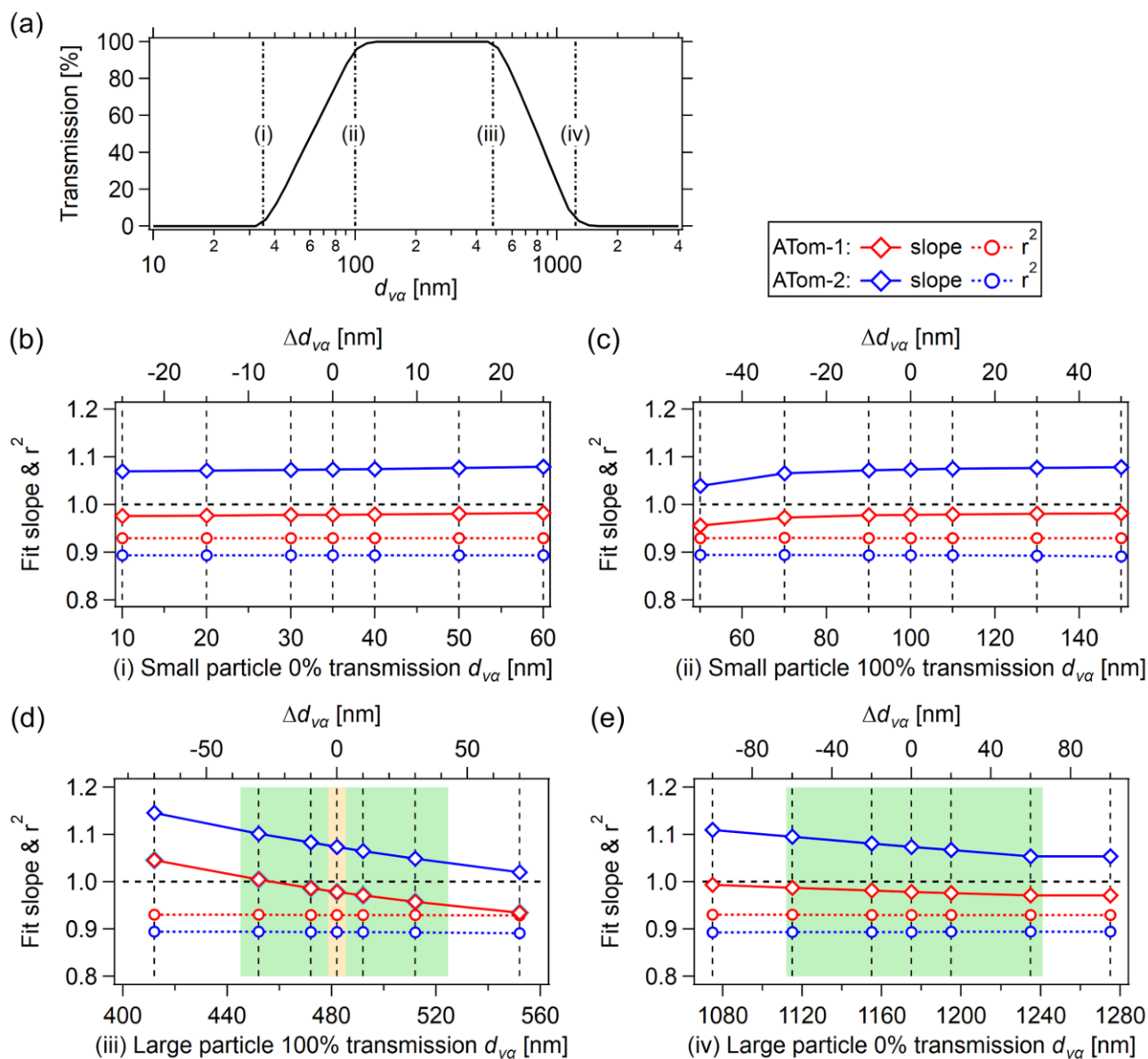
Figure 6: Sensitivity test of AMS transmission: the regression slopes and correlations between V_{chem} (y-axis) and $V_{phys,TC}$ (x-axis) by artificially changing the AMS transmission. The four subpanels labeled with (b), (c), (d), and (e) are for the four anchoring points, (i) 35 nm, (ii) 100 nm, (iii) 482 nm, and (iv) 1175 nm (all in d_{va}), as shown in the top AMS transmission figure. In (d) and (e), the green-tinted background indicates the one standard deviation range from in-field calibrations, and the orange-tinted background in (d) is the narrower standard deviation range estimated from multiple calibrations (Fig. 2).

1237
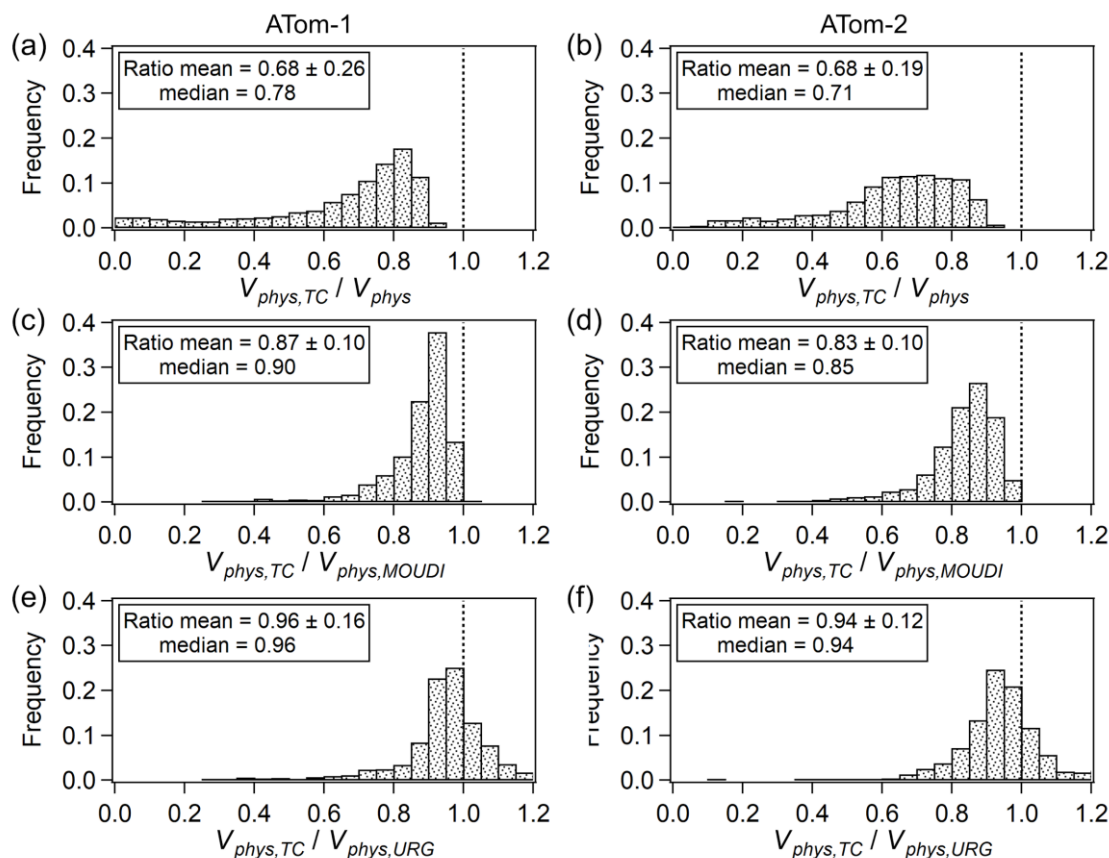
Figure 7: (a-b) Frequency distributions of the AMS-transmission-corrected V_{phys} ($V_{phys,TC}$) vs. the (total) V_{phys}. (c-d) Same for $V_{phys,TC}$ vs. the dry condition altitude-dependent MOUDI-1µm-stage-impactor-transmission-corrected V_{phys} ($V_{phys,MOUDI}$). (e-f) Same for $V_{phys,TC}$ vs. the ground level ambient condition URG-PM$_1$-corrected (standard PM$_1$ cut) V_{phys} ($V_{phys,URG}$). ATom-1 is shown on the left and ATom-2 on the right.

Atmospheric
Measurement
Techniques
Open Access
EGU
Discussions
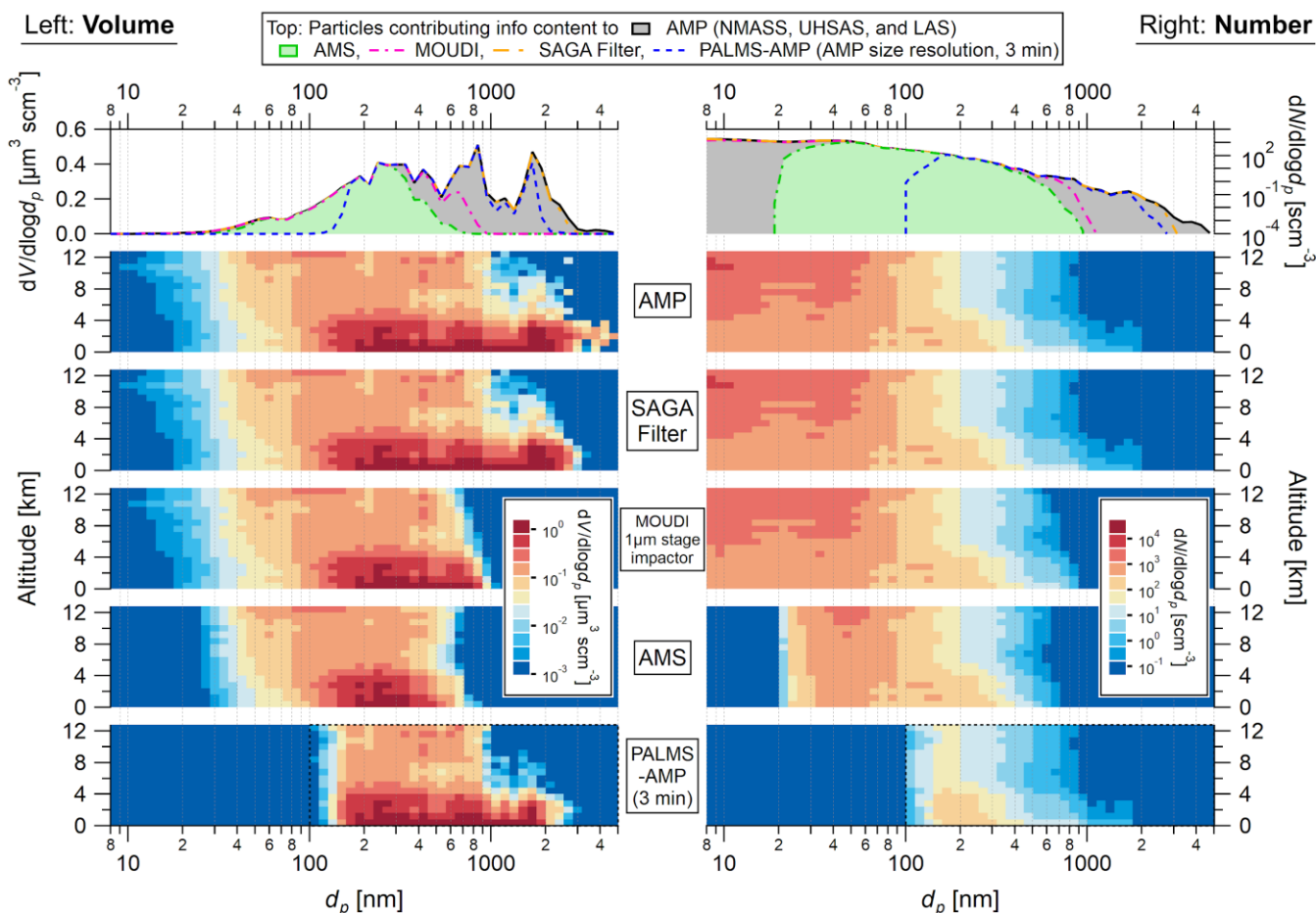
Figure 8: Campaign-averaged volume (left) and number (right) size distributions observed by AMP in ATom-2 (NMASS measured down to 3 nm and here we only show the subrange starting from 8 nm), together with the approximate particle size ranges contributing chemical composition information (without consideration of the details of the chemical detection) to the AMS, PALMS, and SAGA filter, and size-selected by a MOUDI 1 µm stage impactor. The top panel is one dimensional with the campaign average result of each instrument (the transmissions of MOUDI and SAGA filter are altitude dependent and plotted in Fig. 3 and Fig. S18, respectively; PALMS effective detection range depends on counting statistics, and the detected particles given a sampling period are discussed in Fig. S14-15). Note that the top panel shows the fraction of the average, while Fig. 7 shows the average fractions (a summary at Table S2). The right plots represent the size ranges of the number size distribution contributing chemical information to each instrument. The following panels show the vertical profiles of the same quantities for AMP, SAGA filter, MOUDI impactor, AMS, and PALMS-AMP, respectively. The PALMS-AMP product (Froyd et al., 2019) reports composition above 100 nm, the size range indicated by the dashed square in the bottom panels. The plotted altitude bins are 800 m each.
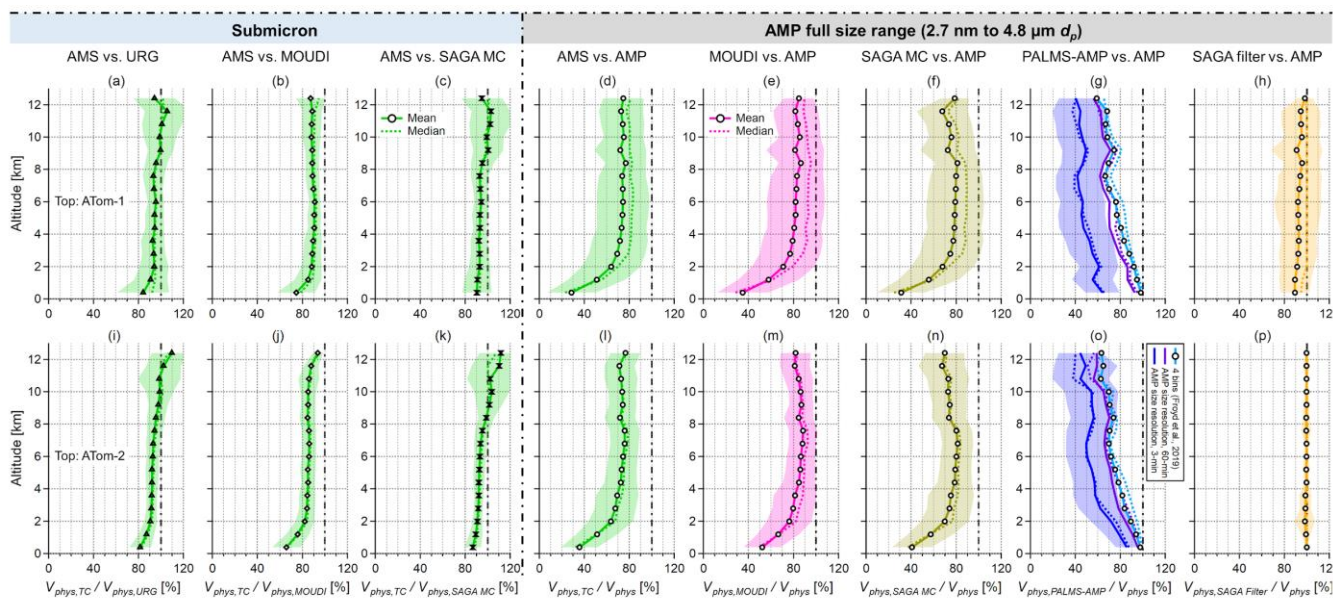
Figure 9: Comparison of the fraction of the particle volume that is observable (i.e., those contributing chemical composition information, but independent of the properties of the chemical detector) between instruments or inlets as a function of altitude, for the conditions in (top) ATom-1 and (bottom) ATom-2. On the left, the widely used approximate submicron cuts are compared. On the right, the ATom aerosol payload is compared, including a MOUDI 1μm impactor that has been flown in other studies. The color-shaded area indicates the SD of volume ratios.